

# Limits on Classical Simulation of Free Fermions with Dissipation

Oles Shtanko,<sup>1,2</sup> Abhinav Deshpande,<sup>1,2</sup> Paul S. Julienne,<sup>2</sup> and Alexey V. Gorshkov<sup>1,2</sup>

<sup>1</sup>Joint Center for Quantum Information and Computer Science,  
NIST/University of Maryland, College Park, Maryland 20742, USA

<sup>2</sup>Joint Quantum Institute, NIST/University of Maryland, College Park, Maryland 20742, USA

Free-fermionic systems are a valuable, but limited, class of many-body problems efficiently simulable on a classical computer. We examine how classical simulability of noninteracting fermions is modified in the presence of Markovian dissipation described by quadratic Lindblad operators, including, for example, incoherent transitions or pair losses. On the one hand, we establish three broad classes of Markovian dynamics that are efficiently simulable classically, by devising efficient algorithms. On the other hand, we demonstrate that, in the worst case, simulating Markovian dynamics with quadratic Lindblad operators is at least as hard as simulating universal quantum circuits. This result is applicable to an experimentally relevant setting in cold atomic systems, where magnetic Feshbach resonances can be used to engineer the desired dissipation. For such systems, our hardness result provides a direct scheme for dissipation-assisted quantum computing with a potential significant advantage in the speed of two-qubit gates and, therefore, in error tolerance.

Understanding whether a particular quantum system is easy or hard to simulate from the perspective of classical computation is a crucial task serving several goals. The first goal, as a primary step of many numerical studies, is to find efficient classical algorithms describing the desired quantum phenomena. Another goal arises in quantum computing, where finding many-body systems lacking an effective classical description may be worthwhile for constructing quantum computation [1] and simulation [2, 3] devices. The versatility of the classical simulability problem can be illustrated by considering the sampling problem for noninteracting and interacting fermions [4–7]. There are efficient classical algorithms to simulate fermions described by a quadratic Hamiltonian: the amplitudes of time-evolved many-body configurations are expressed by an efficiently-computable analytical formula [6, 8]. The existence of an efficient algorithm makes the free-fermion approximation a numerically accessible and valuable method with applications to condensed-matter systems. At the same time, simulating interacting fermions is believed to be classically intractable. Indeed, simulating general interacting fermions is as hard as simulating the output of a universal quantum computer [9]. A similar practical differentiation between easy and hard problems can be applied to other systems [10–14].

In this work, we study the fate of classical simulability of fermionic systems in the presence of dissipation, both for computing local observables and for sampling from the many-body output distribution (to be defined shortly). To obtain a classification of the complexity of simulating free fermions with dissipation, we consider a general class of Markovian processes, i.e. dynamics that depends only on the instantaneous system state and is independent of the preceding evolution [15]. In previous studies, it was shown that adding Markovian single-fermion loss or gain terms keeps the system classically tractable [16, 17]. We show that this result can be generalized to a much wider class of *quadratic-linear* Lindblad operators using the method of stochastic trajectories [18]. At the same time, we also demonstrate that, surprisingly, not all quadratic Lindblad operators are efficiently simulable. In particular, we develop a fermion-based scheme for fault-tolerant universal quantum computation using dis-

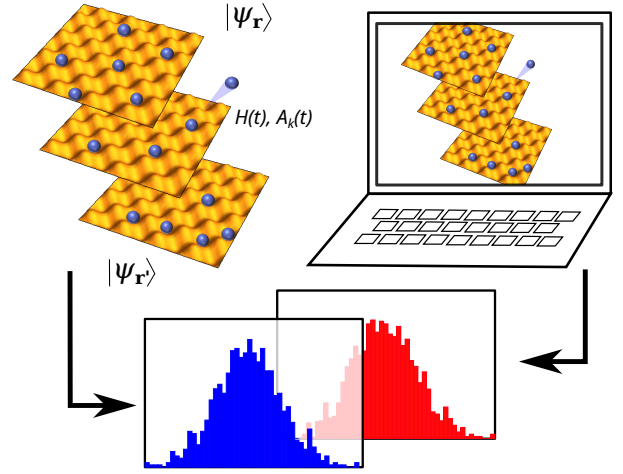


FIG. 1. **Classical simulability.** We look for the existence of an efficient algorithm running on a classical computer and producing (sampling) the many-body configurations with the probability distribution close to the physical system after measurement using some basis. We show that, for fermionic systems with Hamiltonian  $H(t)$  and with dissipation described by quadratic Lindblad operators  $A_k(t)$ , such an algorithm exists for at least a restricted number of problems, while the worst-case scenario requires a quantum computer in order to be solved efficiently. The three optical lattices illustrate the state of the system at initial, intermediate, and final times.

sipative gates exploiting the quantum Zeno effect [19–23]. Therefore, simulating evolution under quadratic Lindblad operators is as hard as simulating an arbitrary quantum computation. The tractability and intractability results together show that simulation of quadratic Lindblad operators is a problem whose complexity can be changed by varying numerical values of one or more parameters in the system, illustrating a complexity phase transition [13].

One motivation behind this work is the existence of a variety of accessible fermionic physical systems involving inelastic processes. Examples of dissipative processes described by quadratic Lindblad operators include two-body loss in trapped alkali atoms [24–26], alkaline-earth atoms [27–32], and cold

molecules [33, 34]. As we will show, Feshbach resonances [35, 36] can be used to significantly suppress coherent interactions between cold atoms, simultaneously increasing the rate of atom-pair trap losses. More general types of dissipation can be created by adding a source of atoms [37–39] or inelastic photon scattering [40–42]. In condensed matter physics, an example of a process that can potentially be described by a Lindblad equation in the Markovian approximation is Cooper-pair loss [43, 44]. Recent progress in the control of dissipative electronic systems has brought them into focus in condensed matter physics. Some of the novel effects in noninteracting and mean-field fermionic systems include dissipation-induced magnetism [45–47], dissipative superfluids and superconductors [48, 49], dissipative Kondo effect [50, 51], non-Hermitian topological phases [52–58], and non-Hermitian localization [59–61].

We provide a classification of dissipative fermionic processes into *easy* (efficiently simulable) and *hard* (not efficiently simulable) classes according to their worst-case computational complexity. The classical simulability problem may be phrased in two ways, either in terms of evaluation of few-body observables or sampling from the full probability distribution on many-body outcomes. In the first task (*few-body observables*), a classical computer is required to output the expectation value of an observable supported on  $k$  sites, where  $k$  does not grow with the system size. In the second task (*sampling*), a classical computer is tasked with producing samples from the same distribution as the one obtained by measuring the time-evolved state in some canonical basis (see Fig. 1). Both tasks allow for the computer to make a small error  $\epsilon$ , measured appropriately in each case [62]. The task of sampling is computationally harder; an algorithm producing samples in some product-state basis can also be used to obtain expectation values of few-body observables in the same basis. Therefore, in this work, we focus mainly on the easiness of sampling in arbitrary product-state bases as a criterion for overall easiness and on the hardness of computing few-body observables as a criterion for overall hardness. This choice gives the stronger of the two results for both easiness and hardness.

We consider dynamics generated by the Lindblad master equation [15, 63]

$$\frac{d\rho}{dt} = -i[H(t), \rho] + \sum_{k=1}^{k_A} A_k(t) \rho A_k^\dagger(t) - \frac{1}{2} \{A_k^\dagger(t) A_k(t), \rho\}, \quad (1)$$

where  $\{X, Y\} \equiv XY + YX$  is the anticommutator,  $\rho(t)$  is the density matrix of the system,  $H(t)$  is a noninteracting Hamiltonian, and  $A_k(t) \in \mathcal{A}(t)$  form a set of  $k_A$  Lindblad operators. We set  $\hbar = 1$  throughout the paper unless specified otherwise. Both the Hamiltonian and the Lindblad operators may depend explicitly on the time but not on the state itself. The corresponding map  $\rho(t_1) = \mathcal{V}(t_1, t_2) \rho(t_2)$  between arbitrary times  $t_1$  and  $t_2 \geq t_1$  satisfies  $\mathcal{V}(t_2, t_1) = \mathcal{V}(t_2, \tau) \mathcal{V}(\tau, t_1)$  for any  $t_2 \geq \tau \geq t_1$ . This divisibility condition is commonly referred to as the most general definition of Markovian dynamics [64]. The master equation in Eq. (1) is invariant under

Type	Examples of $A_k$	Complexity
Dephasing	$c_1^\dagger c_1$	Easy (EC1)
Particle shuffle	$c_1^\dagger c_2$ & $c_2^\dagger c_1$	
Classical fluctuations	$c_1^\dagger$ & $c_1$	
Classical pair fluctuations	$c_1^\dagger c_2^\dagger$ & $c_1 c_2$	
Mixing unitaries	$2c_1^\dagger c_1 - 1 + i(c_2^\dagger + c_2)$	Easy (EC2)
Single-particle loss/gain	$c_1$ OR $c_1^\dagger$	Easy (EC3)
Incoherent hopping	$c_1^\dagger c_2$	Hard
Pair loss/gain	$c_1 c_1$ OR $c_1^\dagger c_1^\dagger$	

TABLE I. Comparison between different types of noninteracting fermion dynamics with additional dissipation. For simplicity, we provide examples for two modes out of  $L$ , denoted by numbers 1 and 2. The symbol & means that both operators are present in the set  $\mathcal{A}(t)$  with factors equal in absolute value. Abbreviations EC1, EC2, EC3 stand for Easy Class 1, 2, and 3 described in the text.

certain transformations of the set of Lindblad operators  $\mathcal{A}(t)$ , such as operator permutations, multiplying any Lindblad operator by a phase factor, or splitting/merging of identical operators as  $A_k \rightleftharpoons \{\sqrt{p}A_k, \sqrt{1-p}A_k\}$ ,  $0 \leq p \leq 1$ .

As a physical system of interest, we consider a fermionic many-body problem where  $N \leq L$  spinless fermions initially occupy  $L$  available levels (modes). Such systems are commonly described by the second quantization method, which expresses any operator, including the Hamiltonian and Lindblad operators, in terms of fermionic Fock operators  $c_n^\dagger$  and  $c_n$ ,  $n \in \{0, 1, \dots, L-1\}$ . Fock operators create and annihilate a single fermion in a particular mode and satisfy the canonical commutation relations  $\{c_n, c_m\} = 0$ ,  $\{c_n^\dagger, c_m\} = \delta_{nm}$ . Though the conventional fermion operators are suitable in most physical problems, in the absence of fermion number conservation it is convenient to use the  $2L$  Hermitian Majorana fermion operators  $\gamma_{2n} = c_n + c_n^\dagger$  and  $\gamma_{2n+1} = -i(c_n - c_n^\dagger)$ , due to their simple anticommutation relations  $\{\gamma_i, \gamma_j\} = 2\delta_{ij}$ ,  $i, j \in \{0, 1, \dots, 2L-1\}$ . We consider the most general form of a noninteracting Hamiltonian [65]

$$H(t) = \frac{i}{2} \sum_{i,j=0}^{2L-1} \alpha_{ij}(t) \gamma_i \gamma_j + \sum_{i=0}^{2L-1} \beta_i(t) \gamma_i, \quad (2)$$

where  $\alpha(t)$  is a real-valued antisymmetric  $2L \times 2L$  matrix and  $\beta(t)$  is a real  $2L$  vector. We assume that the magnitude of all entries of  $\alpha(t)$  and  $\beta(t)$  and their time derivatives scale at most polynomially with system size.

In this work, we focus on the classical resources needed to approximately sample from the fermion distribution at time  $t$ ,

$$P(\mathbf{r}|\mathbf{r}') = \langle \psi_{\mathbf{r}} | \rho(t) | \psi_{\mathbf{r}'} \rangle, \quad \rho(0) = |\psi_{\mathbf{r}'}\rangle \langle \psi_{\mathbf{r}'}|, \quad (3)$$

where  $\mathbf{r}'$  and  $\mathbf{r}$  denote the positions of occupied modes in the initial and final (measured) product-state configurations, respectively, and  $|\psi_{\mathbf{r}}\rangle$  is a product state defined as  $|\psi_{\mathbf{r}}\rangle = c_{r_1}^\dagger \dots c_{r_N}^\dagger |0\rangle = \gamma_{2r_1} \dots \gamma_{2r_N} |0\rangle$ . Importantly, because the dynamics may not conserve the total fermion number, the final number of fermions  $\tilde{N}$  can, in general, be different from the initial number:  $N \neq \tilde{N}$ .

We establish the sufficiency of polynomial resources for classically simulating dynamics due to arbitrary noninteract-

ing Hamiltonians in Eq. (2) and a limited set of Lindblad operators  $A_k(t) \in \mathcal{A}(t)$  in the worst case. In order to prove polynomial-time simulability (also called easiness) for limited classes of dissipative dynamics, we reduce the problem to that of simulating unitary noninteracting fermionic evolution, an easy problem for a classical computer. In order to prove hardness for more general Lindblad operators, we exploit the ability of dissipative dynamics to perform arbitrary quantum computation (i.e. we prove that simulating universal quantum computation reduces to simulating Lindbladian dynamics).

The results of this work are briefly illustrated in Table I. First of all, we define three classically tractable classes of Lindblad operators (defined as Easy Classes 1, 2, and 3). All of these cases allow for polynomial-time sampling of any Hamiltonian and Lindblad operators from the given class on a classical computer, with error scaling inverse-polynomially with  $L$ . Easy Class 1 (EC1) allows for simulation of self-adjoint sets of quadratic Lindblad operators: all Lindblad operators in the set  $\mathcal{A}(t)$  come with their Hermitian conjugate. This class includes such widely used examples as dephasing, incoherent particle shuffle, and classical fluctuations of the number of fermions and of the number of fermion pairs. Easy Class 2 (EC2) works with unitary quadratic Lindblad operators. Finally, Easy Class 3 (EC3) describes the loss or gain of a single particle in the system and can be used in combination with EC1 and/or EC2. At the same time, there exists a class of Lindblad operators with a nonzero measure that is hard to classically simulate. Examples from this class include pair loss/gain and incoherent fermion hopping. Below we explore each class separately.

We focus on quadratic-linear Lindblad operators of the form

$$A_k(t) = \frac{i}{2} \sum_{i,j=0}^{2L-1} a_k^{ij}(t) \gamma_i \gamma_j + \sum_{i=0}^{2L-1} b_k^i(t) \gamma_i + d_k(t) I_{L \times L}, \quad (4)$$

where  $a_k(t)$  and  $b_k(t)$  are arbitrary complex-valued  $L \times L$  matrices and  $L$ -vectors respectively, and  $d_k(t)$  is a number. In this problem, we assume that the number  $k_A$  of nontrivial Lindblad operators from this class is at most  $L(L+1)$ . In fact, any instance where  $\mathcal{A}$  has a larger number of operators can be reduced to a smaller set through a linear transformation [15]. Also, as with the Hamiltonian, we assume that the magnitude of the entries of  $a_k(t)$ ,  $b_k(t)$ , and  $d_k(t)$  and their time derivatives grow at most polynomially with the system size.

This work is organized as follows. In Section I, we provide a brief introduction to free-fermion sampling, recalling established results in the literature and connecting them to the most general form of quadratic-linear Hamiltonians. In Section II, we derive three new algorithms allowing us to solve distinct classes of fermionic problems involving quadratic Lindblad operators and prove that these algorithms run in time that is polynomial in both  $L$  and the inverse of the distance from the exact distribution. In Section III, we establish examples that belong to the hard class and show their robustness to the presence of minor imperfections. Finally, in Section IV, we provide an explicit cold-atom proposal for realizing a model from the hard class. This cold-atom proposal, in fact, serves as a quantum computing architecture.

## I. FREE-FERMION SAMPLING

In this Section, we discuss the noninteracting fermion problem in the absence of dissipation. We recap the work of Terhal and DiVincenzo [6], which shows that all output probabilities  $P(\mathbf{r}|\mathbf{r}')$  in Eq. (3) and the marginal probabilities can be obtained using a classically tractable analytical formula. Before referring to this result, we need to incorporate the linear terms present in Eq. (2) into effective quadratic dynamics. In order to do so, we consider a slightly larger system containing an extra ancilla  $(L+1)$ th mode [65], labeled as  $n = L$ . Next, we choose new effective dynamics such that the ancilla mode remains in the state  $|+\rangle \equiv (|0\rangle + |1\rangle)/\sqrt{2}$  during the entire evolution, including the initial and final times, i.e.

$$|\psi_{\mathbf{r}'}\rangle \rightarrow |\psi_{\mathbf{r}'}\rangle \otimes |+\rangle, \quad |\psi_{\mathbf{r}}\rangle \rightarrow |\psi_{\mathbf{r}}\rangle \otimes |+\rangle. \quad (5)$$

To construct such dynamics, we consider a new Hamiltonian by replacing  $\gamma_i \rightarrow i\gamma_i\gamma_{2L}$ , where  $\gamma_{2L}$  and  $\gamma_{2L+1}$  are Majorana operators acting on the ancilla mode. It is straightforward to check that such a transformation results in a new purely quadratic Hamiltonian (without any linear terms) that keeps the state of the ancilla stationary and does not modify the dynamics of the original Hamiltonian. The new coefficients in Eq. (2) are

$$\alpha_{ij} \rightarrow \tilde{\alpha}_{ij} = \alpha_{ij} + \delta_{i2L+2}\beta_j - \delta_{j2L+2}\beta_i, \quad (6)$$

where we use by default  $\beta_{2L} = \beta_{2L+1} = 0$ . Given that the modified initial and final conditions for the system and the ancilla are  $\{\mathbf{r}'\} \rightarrow \{\mathbf{r}', s'\}$ ,  $\{\mathbf{r}\} \rightarrow \{\mathbf{r}, s\}$ ,  $s, s' \in \{0, 1\}$ , the probability  $P(\mathbf{r}|\mathbf{r}')$  of obtaining outcome  $\mathbf{r}$  for the original system can be computed from the probability  $P(\{\mathbf{r}, s\}|\{\mathbf{r}', s'\})$  for the system with the ancilla as follows:

$$P(\mathbf{r}|\mathbf{r}') = \frac{1}{2} \sum_{s, s' \in \{0, 1\}} P(\{\mathbf{r}, s\}|\{\mathbf{r}', s'\}). \quad (7)$$

Summarizing, this method ensures that the dynamics of a linear-quadratic Hamiltonian can always be reduced to the dynamics of a quadratic one by expanding the system size by one mode. Therefore, we henceforth consider only quadratic Hamiltonians.

Let us derive the formula for the sampling probability. We start from a (backwards) time-evolved Majorana fermion operator  $\gamma_i(t) = U_t \gamma_i U_t^\dagger$ , where  $U_t = \mathcal{T} \exp(-i \int_0^t H(t') dt')$ . Given the quadratic structure of the Hamiltonian, this evolution is a linear transformation  $\gamma_i(t) = \sum_j R_{ij}(t) \gamma_j$ , where  $R = \mathcal{T} \exp(-2 \int_0^t \alpha(t') dt')$  is a unitary  $2L \times 2L$  matrix. One can use this expression to derive the time evolution of a fermion operator as

$$U_t c_n U_t^\dagger = \frac{1}{2} U_t (\gamma_{2n} + i\gamma_{2n+1}) U_t^\dagger = \sum_j T_{nj} \gamma_j, \quad (8)$$

where  $T_{nj} \equiv R_{2n,j} + iR_{2n+1,j}$  are elements of a  $L \times 2L$  transformation matrix  $T$ . Labeling the initially empty sites as  $l'_i$  and recalling that the initial fermion positions are  $r'_i$  and

that the final positions are  $r_i$ , the linearity allows to write the output probability in Eq. (3) at any time as

$$\begin{aligned} P(\mathbf{r}|\mathbf{r}') &= \langle \psi_{\mathbf{r}} | U_t | \psi_{\mathbf{r}'} \rangle \langle \psi_{\mathbf{r}'} | U_t^\dagger | \psi_{\mathbf{r}} \rangle \\ &= \langle \psi_{\mathbf{r}} | U_t c_{r'_1}^\dagger c_{r'_1} \dots c_{l'_{L-N}}^\dagger c_{l'_{L-N}} U_t^\dagger | \psi_{\mathbf{r}} \rangle \\ &= \sum_{n_1, \dots, n_L; m_1, \dots, m_{L-N}} T_{r'_1 n_1}^* T_{r'_1 m_1} \dots T_{l'_{L-N} m_L} T_{l'_{L-N} n_L}^* \times \\ &\quad \langle 0 | \gamma_{2r_N} \dots \gamma_{2r_1} \gamma_{n_1} \gamma_{m_1} \dots \gamma_{m_L} \gamma_{n_L} \gamma_{2r_1} \dots \gamma_{2r_N} | 0 \rangle. \end{aligned} \quad (9)$$

This expression can be computed efficiently using Wick's theorem and written in a compact form. Let  $\mathcal{I}$  be a subset of indices with increasing order and  $A[\mathcal{I}]$  be the matrix whose elements satisfy  $A[\mathcal{I}]_{ij} \equiv A_{\mathcal{I}_i, \mathcal{I}_j}$ . Consider the set  $\mathcal{I} = \{r'_i, L + l'_j, 2L + 2r_k\}$ , where  $i \in \{1, 2, \dots, N\}$ ,  $j \in \{1, 2, \dots, L - N\}$ , and  $k \in \{1, 2, \dots, \tilde{N}\}$  take all possible values. Then the result can be written as [6]

$$P(\mathbf{r}|\mathbf{r}') = \text{Pf } M[\mathcal{I}], \quad (10)$$

where Pf is the Pfaffian, and  $M$  is a  $4L \times 4L$  matrix

$$M = \begin{pmatrix} T\Lambda T^T & T\Lambda T^\dagger & T\Lambda \\ T^*\Lambda T^T & T^*\Lambda T^\dagger & T^*\Lambda \\ \Lambda T^T & \Lambda T^\dagger & I \end{pmatrix}, \quad (11)$$

where, in turn, the  $2L \times 2L$  matrix  $\Lambda$  is

$$\Lambda = I_{L \times L} \otimes \begin{pmatrix} 1 & i \\ -i & 1 \end{pmatrix}. \quad (12)$$

The expression in Eq. (10) can be efficiently evaluated on a classical computer using existing polynomial-time algorithms for computing Pfaffians [8]. Similarly, marginal probabilities can be efficiently computed conditioning on the output of a given fraction of sites, as in Ref. [6], which is enough to efficiently sample from the output probability distribution.

## II. EASY CLASSES

Here we present three algorithms that allow simulating specific fermionic problems involving quadratic Hamiltonians and quadratic-linear Lindblad operators. All methods are based on stochastic unraveling, i.e., replacing dissipative dynamics by a stochastic free-fermion Hamiltonian without changing the outcome distribution. Since each stochastic realization can be simulated efficiently by a classical computer, as established in the previous section, a classical computer can serve as a black box sampler that reproduces measured outcomes. In this Section, we demonstrate that the classes of problems belonging to the aforementioned Easy Classes 1–3 are efficiently simulable. In particular, we show that these problems require computation resources  $C$  (number of operations) bounded as  $C \leq \text{poly}(L, t^2/\epsilon)$  to sample from a distribution that is  $\epsilon$ -close to the target distribution. Therefore, we establish efficient classical algorithms for approximate dissipative fermion sampling in the presence of certain classes of quadratic-linear Lindblad operators.

### A. Efficient classical algorithms

Let us define *Easy Class 1* (EC1) as problems that involve quadratic-linear self-adjoint Lindblad sets  $\mathcal{A}(t)$  defined as follows. We assume that at any time one can divide the set as a union of two equal-size subsets,  $\mathcal{A} = \mathcal{A}_1 \cup \mathcal{A}_2$ , where the Hermitian conjugate of every Lindblad operator in  $\mathcal{A}_1$  returns an operator in  $\mathcal{A}_2$  (and vice versa). Under this division, any Hermitian Lindblad operator must be included in both subsets  $\mathcal{A}_1$  and  $\mathcal{A}_2$  with normalization factor  $1/\sqrt{2}$ . The latter splitting can be seen as a transformation that keeps the Lindblad equation invariant, as defined earlier below Eq. (1). Examples from EC1 include several important physical models such as dephasing and classical fluctuations (see examples of sets in lines 1–4 in Table I).

To efficiently simulate dynamics from EC1, we consider a stochastic Hamiltonian

$$H'(t) = H(t) + \sum_{A_k \in \mathcal{A}_1} \theta_k(t) A_k(t) + \theta_k^\dagger(t) A_k^\dagger(t), \quad (13)$$

where  $\theta_k(t)$  is a complex random variable taking constant values  $\theta_k(t) = \xi_{nk}/\sqrt{\Delta\tau}$  during short time intervals  $t \in [n\Delta\tau, (n+1)\Delta\tau]$ . The discrete complex Gaussian variables  $\xi_{nk}$  satisfy  $\mathbb{E}\xi_{nk} = 0$ ,  $\mathbb{E}\xi_{nk}^* \xi_{n'k'} = \delta_{nn'} \delta_{kk'} \delta_{ab}$ . We assume that the timestep  $\Delta\tau$  is small. Then, given a stochastic Hamiltonian of the form in Eq. (13), the original dynamical map  $\mathcal{V}(t_2, t_1)$  generated by the Lindblad equation can be approximated as

$$\mathcal{V}(t_2, t_1) = \mathbb{E}\mathcal{V}_{\text{st}}(t_2, t_1) + \delta\mathcal{V}(t_2, t_1)\Delta\tau + O(\Delta\tau^2), \quad (14)$$

where  $\delta\mathcal{V}(t_2, t_1)\Delta\tau$  is the lowest-order correction (to be explicitly derived below) and  $\mathcal{V}_{\text{st}}$  is a stochastic unitary map

$$\mathcal{V}_{\text{st}}(t_2, t_1)\rho = U(t_2, t_1)\rho U^\dagger(t_2, t_1). \quad (15)$$

In the above,  $U(t_2, t_1) = \mathcal{T} \exp(-i \int_{t_1}^{t_2} dt' H'(t'))$  encodes the time-evolution due to  $H'(t)$  in Eq. (13). The average  $\mathbb{E}$  in Eq. (14) is taken over the stochastic fields  $\theta_k(t)$ . The resulting output probabilities satisfy

$$P(\mathbf{r}|\mathbf{r}') = \mathbb{E} P_{\text{st}}(\mathbf{r}|\mathbf{r}') + O(\Delta\tau), \quad (16)$$

where  $P_{\text{st}}(\mathbf{r}|\mathbf{r}')$  is the output probability for the unitary dynamics in Eq. (15) obtained via the formula in Eq. (10). Therefore, a computer programmed to sample from the distribution for a randomly chosen set of unitary trajectories will produce outcomes with the same probabilities as the physical process following Lindbladian evolution, up to  $O(\Delta\tau)$  error. The cost of suppression of this error in terms of computational resources will be discussed later in this section. Here we just specify that the correction to the dynamical map, which we treat as an error, can be expressed as

$$\delta\mathcal{V}(t_2, t_1) = \mathbb{E} \int_{t_1}^{t_2} dt' \mathcal{V}_{\text{st}}(t_2, t') \mathcal{D}(t') \mathcal{V}_{\text{st}}(t', t_1), \quad (17)$$

where  $\mathcal{D}(t)$  is a time-local superoperator

$$\mathcal{D}(t)\rho = \sum_{\alpha} D_{\alpha}^{(1)}(t)\rho D_{\alpha}^{(2)}(t). \quad (18)$$



Here, the operators  $D_\alpha^{(i)}(t) = \text{poly}_4(H(t), A_k(t))$  can be expressed as polynomials of degree four in terms of the Hamiltonian and Lindblad operators at time  $t$ . Therefore,  $D_\alpha^{(i)}(t)$  can always be presented as a sum of terms, each being a product of no more than eight Majorana operators. The specific form of these operators and the derivation of Eq. (14) can be found in Appendix A.

Let us consider another class of problems, *Easy Class 2* (EC2), that include unitary quadratic Lindblad operators  $A_k = \sqrt{\Gamma_k(t)} Y_k(t)$ , where  $\Gamma_k(t) \geq 0$  are time-dependent rates and  $Y_k(t) = \exp(-iG_k(t))$  are unitary operators generated by quadratic-linear Hamiltonians  $G_k(t)$  of the form in Eq. (2). To classically simulate dynamics under EC2, we also consider discretized time evolution with sufficiently small timesteps  $\Delta\tau$  and set the unitary transformation  $U(t_1, t_2) = \prod_{n=n_1}^{n_2} U_n$ , where the timestep unitaries  $U_n$  are generated randomly according to the rule

$$U_n = U_n^0 \times \begin{cases} Y_k(t_n), & p_k = \Gamma_k(t_n)\Delta\tau, \\ I, & p_0 = 1 - \sum_k \Gamma_k(t_n)\Delta\tau. \end{cases} \quad (19)$$

Here  $p_k$  are probabilities that are used to generate the respective outcomes,  $U_n^0 = \mathcal{T} \exp(-i \int_{n\Delta\tau}^{(n+1)\Delta\tau} H(t) dt)$ , and  $t_n \in [n\Delta\tau, (n+1)\Delta\tau]$  are random times generated from the uniform distribution.

Notwithstanding the slightly different stochastic unraveling, the procedure for approximating EC2 is the same as for EC1. In particular, the system dynamics is described by the expression in Eq. (14) leading to the distribution in Eq. (16), with the average taken over stochastic unitary realizations. The correction term has the form in Eq. (18), but the operators  $D_\alpha^{(i)}(t)$  here are degree-two polynomials in the Hamiltonian and Lindblad operators. The detailed form of the operators along with the derivation can be found in Appendix B.

Finally, let us consider *Easy Class 3* described by generic linear Lindblad operators  $A_k(t) = \sum_i b_k^i \gamma_i + d_k I_{L \times L}$ , which can be obtained by setting  $a_k = 0$  in Eq. (4) without assuming any additional restrictions on the set  $\mathcal{A}(t)$ . The simulation of dynamics under this class uses the same method as EC1 but requires a presence of  $L_a = t/\Delta\tau$  ancilla fermion modes corresponding to the number of time steps. Let us enumerate the ancilla modes described by Majorana fermion operators  $\gamma_{2n}$  and  $\gamma_{2n+1}$  using indices  $n = L, \dots, L + L_a - 1$ . We also assume that the ancilla modes are initialized in the vacuum state and traced out after performing the evolution. The dynamics of both the system and the ancillas can be described as unitary evolution with the Hamiltonian in Eq. (13), with one important difference. Now, the quantities  $\theta_k(t)$  in the time interval  $t \in [n\Delta\tau, (n+1)\Delta\tau]$  are operators instead of numbers, and are given by

$$\theta_k(t) = \xi_{nk} \Delta\tau^{-1/2} (\gamma_{2(L+n-1)} + i\gamma_{2(L+n)-1}). \quad (20)$$

The random variables  $\xi_{nk}$  are the same as in EC1. The idea is that we pair a loss (gain) term on the system with a gain (loss) term on the ancilla to make the overall Hamiltonian quadratic. After discarding the ancilla modes, the evolution becomes equivalent to the target dissipative dynamics, up to

a discretization error that originates from the approximation in Eq. (14) and Eq. (18), with  $D_\alpha^{(i)}(t)$  expressed as degree-four polynomials in the Hamiltonian and Lindblad operators, as shown in Appendix C.

## B. Performance of the classical algorithms

Let us quantify the error of the method of quantum trajectories used for Easy Classes 1–3, and then show that the sampled distribution can be made arbitrarily close to the exact one with an appropriate choice of the timestep  $\Delta\tau$ . In order to characterize the approximation error  $\epsilon$  associated with sampling from a distribution  $\tilde{P}(\mathbf{r}|\mathbf{r}')$  different from the ideal distribution  $P(\mathbf{r}|\mathbf{r}')$ , we utilize the total variation distance

$$\epsilon = \frac{1}{2} \max_{\mathbf{r}'} \sum_{\mathbf{r}} |\tilde{P}(\mathbf{r}|\mathbf{r}') - P(\mathbf{r}|\mathbf{r}')|, \quad (21)$$

where the maximization is over all possible initial product-state configurations  $\mathbf{r}'$ .

Using convexity of the absolute value and the expression for the correction in Eqs. (17)–(18), the error can be bounded as (see Appendix D),

$$\epsilon \leq \frac{\Delta\tau}{2} \max_{\mathbf{r}'} \sum_{\alpha} \int_0^t dt' C_{\mathbf{r}'}^{\alpha}(t, t') + O(\Delta\tau^2), \quad (22)$$

where

$$C_{\mathbf{r}'}^{\alpha}(t, t') = \mathbb{E} \sum_{\mathbf{r}} \left| \langle \mathbf{r} | D_{\alpha}^{(1)}(t, t') \rho_{\mathbf{r}'}(t) D_{\alpha}^{(2)}(t, t') | \mathbf{r} \rangle \right|. \quad (23)$$

Here  $D_{\alpha}^{(i)}(t, t') = \mathcal{V}_{\text{st}}(t, t') D_{\alpha}^{(i)}(t')$  and  $\rho_{\mathbf{r}'}(t) = \mathcal{V}_{\text{st}}(t, 0) \rho_{\mathbf{r}'}$  are operators transformed according to unitary evolution for a single stochastic trajectory, and the average  $\mathbb{E}$  is taken over all trajectories. We now use the following lemma to further bound this expression.

**Lemma.** Consider two sparse operators  $O_1$  and  $O_2$  whose matrix elements satisfy

$$\langle \mathbf{r} | O_{\alpha} | \mathbf{r}' \rangle = 0 \quad \text{if} \quad d_H(\mathbf{r}, \mathbf{r}') \geq k_{\alpha}, \quad \alpha \in \{1, 2\}, \quad (24)$$

where  $d_H$  is the Hamming distance, and  $\mathbf{r}, \mathbf{r}'$  are binary strings of length  $L$  representing computational basis states. Let  $\rho$  be a normalized positive semidefinite operator,  $\rho \geq 0$ ,  $\text{Tr} \rho = 1$ , then

$$\sum_{\mathbf{r}} |\langle \mathbf{r} | O_1 \rho O_2 | \mathbf{r} \rangle| \leq \frac{L^{k_1+k_2}}{k_1! k_2!} \|O_1\|_{\max} \|O_2\|_{\max}, \quad (25)$$

where  $\|O_{\alpha}\|_{\max}$  is the max-norm.

The proof of the Lemma can be found in Appendix D. The result of the Lemma allows us to simplify Eq. (23) as

$$C_{\mathbf{r}'}^{\alpha}(t, t') \leq \frac{L^{k_{1\alpha}+k_{2\alpha}}}{k_{1\alpha}! k_{2\alpha}!} \|D_{\alpha}^{(1)}(t, t')\|_{\max} \|D_{\alpha}^{(2)}(t, t')\|_{\max}, \quad (26)$$

where  $k_{i\alpha}$  is the locality of the operator  $D_\alpha^{(i)}(t, t')$ , i.e. the maximum number of Majorana operators in its decomposition. Because  $\mathcal{V}_{\text{st}}$  is a map describing free-fermion evolution, the locality  $k_{i\alpha}$  of the operator  $D_\alpha^{(i)}(t, t')$  is equal to the locality of  $D_\alpha^{(i)}(t')$ . At the same time, as analyzed in the previous section, the localities of operators  $D_\alpha^{(i)}(t')$  satisfy  $k_{\mu\alpha} \leq k_m$ , where  $k_m = 8$  for EC1/EC3, and  $k_m = 4$  for EC2. We can also bound the max-norm by the (spectral) operator norm

$$\|D_\alpha^{(i)}(t, t')\|_{\max} \leq \|D_\alpha^{(i)}(t, t')\| = \|D_\alpha^{(i)}(t')\|. \quad (27)$$

As a result, the error bound is given by

$$\epsilon \leq \frac{\Delta\tau}{2} \frac{L^{2k_m}}{(k_m!)^2} \sum_\alpha \int_0^t dt' \|D_\alpha^{(1)}(t')\| \|D_\alpha^{(2)}(t')\|. \quad (28)$$

Since the matrices  $D_\alpha^{(i)} = \text{poly}(H, A_k)$  are generated by a quadratic-linear Hamiltonian  $H$  and set of Lindbladians  $A_k$ , we can always find a polynomially large bound for the norm  $\|D_\alpha^{(i)}(t')\| \leq \text{poly}(L)$ . Thus, there always exists a discretization step

$$\Delta\tau \leq \frac{\epsilon}{t \text{ poly}(L)} \quad (29)$$

that keeps the error in Eq. (28) arbitrarily small, suppressed at least polynomially with the number of modes  $L$ .

Let us now estimate the amount of computational resources required to perform the above sampling procedure. For each sample, the algorithm randomly chooses a unitary trajectory according to the given prescription for each class EC1–EC3 and, according to the Terhal-DiVincenzo algorithm, samples outputs from the free-fermion distribution in Eq. (10). In particular, it samples the output at site  $i$  conditioned upon the outcomes sampled at sites  $j < i$ , for which the marginal probabilities should also be computed. Consider cases of EC1 and EC2 that do not require ancillas. Once the matrix  $T$  is obtained in Eq. (8), the number of steps to compute the distribution is equal to  $C' = L \times O(L^3) = O(L^4)$ , where the factor  $O(L^3)$  is the upper bound on the time it takes to compute a Pfaffian of an  $O(L) \times O(L)$  matrix. Further, the runtime for obtaining the matrix  $T$  is proportional to  $t/\Delta\tau \times M(2L)$ , where  $M(n) \lesssim O(n^3)$  is the time for  $n \times n$  matrix multiplication. In sum, the total bound on the runtime for each trajectory is bounded as  $C \sim O(L^4) + O(L^3 t/\Delta\tau)$ . Choosing  $\Delta\tau = \epsilon/(t \times \text{poly}(L))$ , the runtime is

$$C \leq \text{poly}\left(L, \frac{t^2}{\epsilon}\right). \quad (30)$$

For EC3, the derivation is the same up to adjusting the system size to include the ancilla modes,  $L \rightarrow L + t/\Delta\tau$ . This case also has a similar polynomial upper bound on the classical runtime in the form of Eq. (30) as long as the evolution time  $t$  is polynomial.

### III. HARD CLASS

We have so far demonstrated cases when the probability distribution generated by the Lindblad equation is efficiently

simulable on a classical computer. Can we extend these proofs to the most general case of quadratic  $A_k$ 's? Since quadratic operators  $A_k$  correspond to single-fermion jumps in many cases, one may expect that the problem can be solved in the single-particle sector, similar to unitary free-fermion dynamics. However, such an intuition is incomplete. A simple explanation can be obtained using the Fermi exclusion principle that requires the transition between two modes to depend on the occupation of the target mode; thus a quadratic Lindbladian jump operator can induce many-body correlations in the system that quickly become classically intractable.

#### A. Reduction to a generic quantum circuit

We now provide a rigorous argument for worst-case hardness based on the equivalence of dynamics under classes  $H(t)$  and  $A_k(t)$  in Eq. (1) on the one hand and universal quantum computing on the other. Let us start with the simplest map utilizing quadratic Hamiltonians. We distribute all modes into  $L/2$  pairs, each pair corresponding to a logical qubit in the state  $|0\rangle_L = |01\rangle$  or  $|1\rangle_L = |10\rangle$ . Then, utilizing only quadratic Hamiltonians and Lindblad operators, we can implement any quantum circuit with arbitrary precision. Thus, by showing the equivalence of the dynamics to universal quantum computation, we obtain hardness results for both estimating time-evolved local observables  $\langle O(t) \rangle$  and sampling from the time-evolved state in any local basis. The obtained hardness result is therefore on par with the best complexity-theoretic evidence that simulating quantum circuits (in both senses) is hard.

First, using single-fermion hopping between the two sites of a qubit, we can reproduce arbitrary single-qubit operations [66]. Second, to approximately generate a desired two-qubit gate, we can use hopping combined with a quadratic Lindblad operator. In particular, assigning the two-qubit logical states  $|00\rangle_L = |0101\rangle$ ,  $|01\rangle_L = |0110\rangle$ ,  $|10\rangle_L = |1001\rangle$ , and  $|11\rangle_L = |1010\rangle$ , the control-Z gate can be implemented by simultaneously applying the hopping Hamiltonian  $H = J(c_2^\dagger c_3 + c_3^\dagger c_2)$  and pair-loss operator  $A = \Gamma c_3 c_4$  for time  $t = \pi/J$ , in the limit  $\Gamma \gg J$ . This type of dynamics can be analyzed as follows. The logical states  $|01\rangle_L$  and  $|10\rangle_L$  remain invariant in the course of the evolution. At the same time, in the limit  $\gamma \equiv \Gamma/J \rightarrow \infty$ , due to the quantum Zeno effect, the Lindblad operator's action disallows any coherent transition involving states where qubits 3 and 4 are both occupied (i.e.  $|\cdot \cdot 11\rangle$ ). As a result, the logical state  $|00\rangle_L$  is unaffected by the evolution. Therefore, the only evolving logical state is  $|11\rangle_L$ , which acquires a phase factor  $\exp(i\pi) = -1$  after time  $t = \pi/J$ . As a result, the effective transformation on the two logical qubits is the control-Z gate

$$|\psi\rangle \rightarrow U_\pi |\psi\rangle, \quad U_\pi = \begin{pmatrix} 1 & 0 & 0 & 0 \\ 0 & 1 & 0 & 0 \\ 0 & 0 & 1 & 0 \\ 0 & 0 & 0 & -1 \end{pmatrix}. \quad (31)$$

Together with arbitrary single-qubit operations, the control-Z gate is enough to obtain dynamics universal for quantum

computing and hence hard to approximately sample from, assuming standard conjectures in complexity theory [67, 68].

Importantly, the performance of the dissipative gate relies on the Zeno-effect blockade effective for  $\gamma \rightarrow \infty$ . In the limit of large but finite  $\gamma$ , the two-qubit system has the probability  $\epsilon = 2\pi/\gamma + O(\gamma^{-2})$  of ending up in states  $|0011\rangle$  or  $|0000\rangle$ , which could result in an error in the gate (see Appendix E). To avoid computational error, we can choose the ratio  $\gamma$  to be arbitrarily large by taking vanishing  $J \rightarrow \text{poly}^{-1}(L)$  for any given  $\Gamma > 0$ . Therefore, we can keep the error below any given threshold at the cost of increased overall computation time, which remains polynomial in system size.

The proposed architecture is not unique and allows for modified/generalized realizations of logical qubits and gates. For example, if the pair decay is always present on any two neighboring modes, one may introduce an empty ancilla mode between two logical qubits in order to ensure that logical states don't decay. As another example, if the control Hamiltonian is linear in terms of Majorana operators, a logical qubit can be encoded using just a single mode. Moreover, for a reader focused on applications, we discuss below a practical modification of qubit encoding implementable in cold atoms.

In addition, pair loss can also be replaced by other types of dissipation. To demonstrate this, consider an arbitrary free-fermion unitary transformation  $Y(t) = \exp(-iG(t))$ , where  $G(t)$  belongs to the quadratic-linear class in Eq. (2). Then the entangling gate can always be realized using Lindblad operators  $A' = \Gamma Y(t)c_1c_2Y^\dagger(t)$  and a free-fermion Hamiltonian. Indeed, by replacing  $A$  with  $A'(t)$ ,  $H(t)$  with  $H'(t) = Y^\dagger(t)H(t)Y(t)$ , and applying  $Y(0)^\dagger$  and  $Y(t)$  to the initial and final states, we get an equivalent process with the same probability distribution. Since  $Y(t)$  generates free-fermion dynamics, this new process is equivalent to a new scheme utilizing dissipation  $A'(t)$ . As a result, Lindbladians such as incoherent transitions  $A = \Gamma c_1^\dagger c_2$  or pair gains  $A = \Gamma c_1^\dagger c_2^\dagger$  can also be used for quantum computing. Therefore, these problems belong to the hard class (see Table I). We now discuss the tolerance of this result to perturbations.

### B. Robustness of the hardness result

The error associated with imperfect Zeno blockade cannot be arbitrarily suppressed by slowing down the computation if there are small generic corrections to the dissipative dynamics. These corrections can be viewed as the presence of additional Lindblad operators with total rate  $\Gamma'$ . Such terms generate additional transitions with the probability  $\epsilon' \sim \pi\Gamma'/J$ , where  $\Gamma'$  is the combined rate of added operators  $A'$  and/or other errors. In contrast to the imperfect-Zeno-blockade error, this type of error diverges for small  $J$ . Therefore, there is an optimal value  $J \sim \sqrt{\Gamma'/\Gamma}$  that minimizes the overall gate error to  $\epsilon + \epsilon' \sim O(1)$ , including, besides standard errors, *leakage* into states outside of the logical Hilbert space. For fixed  $\Gamma$ , there always exists a choice of  $\Gamma' \sim O(1)$  that keeps the error below any provided threshold,  $\epsilon + \epsilon' < p_0$ , where  $p_0 > 0$ . According to the leakage threshold theorem in Ref. [69], which is a generalization of earlier standard thresh-

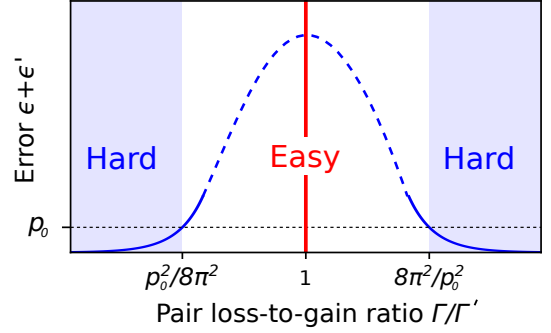


FIG. 2. **Complexity phase diagram for a fermionic system with simultaneous pair losses and gains.** The plot illustrates the connection between complexity of simulation and the hypothetical dissipative control-Z gate error  $\epsilon + \epsilon'$  (both axes use log scale). When the error is smaller than the best-known two-qubit error-correction threshold  $p_0$ , the worst-case system dynamics is equivalent to that of a fault-tolerant quantum computer (blue shaded regions) and, according to existing complexity conjectures, is classically computationally hard to simulate. In contrast, when the rates of gain and loss are exactly equal, the problem belongs to EC1 (vertical red line) with the effective classical algorithm provided in the text. The result for the unshaded region remains inconclusive. The dashed line represents qualitative extrapolation.

old results [70–72], a universal set of such gates can be used to implement fault-tolerant quantum computing. Therefore, there are instances of Lindblad evolutions that remain hard to simulate for arbitrarily long times.

One particular example of a dissipative correction to ideal dynamics is the presence of pair gain  $A'_{ij} = \Gamma' c_i^\dagger c_j^\dagger$  that acts on exactly the same sites as pair loss  $A_{ij}$ . In this case, the minimum error is  $\epsilon + \epsilon' = \sqrt{8\pi^2\Gamma'/\Gamma}$  and the problem remains hard for a classical computer if  $\Gamma' \leq p_0^2/8\pi^2\Gamma$ . Since the entangling gate is also implementable using pair gain instead of loss, this inequality also works after replacing  $\Gamma$  by  $\Gamma'$ . Thus, the problem of simulating the evolution in the regions  $\Gamma'/\Gamma \leq p_0^2/8\pi^2$  and  $\Gamma'/\Gamma \geq 8\pi^2/p_0^2$  is classically hard. The complexity for the rest of parameter space remains an open problem. Notably, there exists at least one point in this range,  $\Gamma = \Gamma'$ , that is easily simulable by a classical computer since it is in EC1. Therefore, by changing the ratio  $\Gamma'/\Gamma$ , we can potentially induce a complexity phase transition. Figure 2 illustrates the connection between gate error and sampling complexity.

## IV. APPLICATION TO COLD ATOMS

In this section, we discuss the application of hardness results from the previous sections to experiments utilizing cold atoms. In particular, we demonstrate that pair loss can be significantly amplified in cold atomic systems by a magnetic Feshbach resonance, empowering the use of dissipation as a tool for constructing entangling gates. In such systems, the hardness results lead to the possibility of implementing quantum circuits using pair loss instead of unitary interactions.

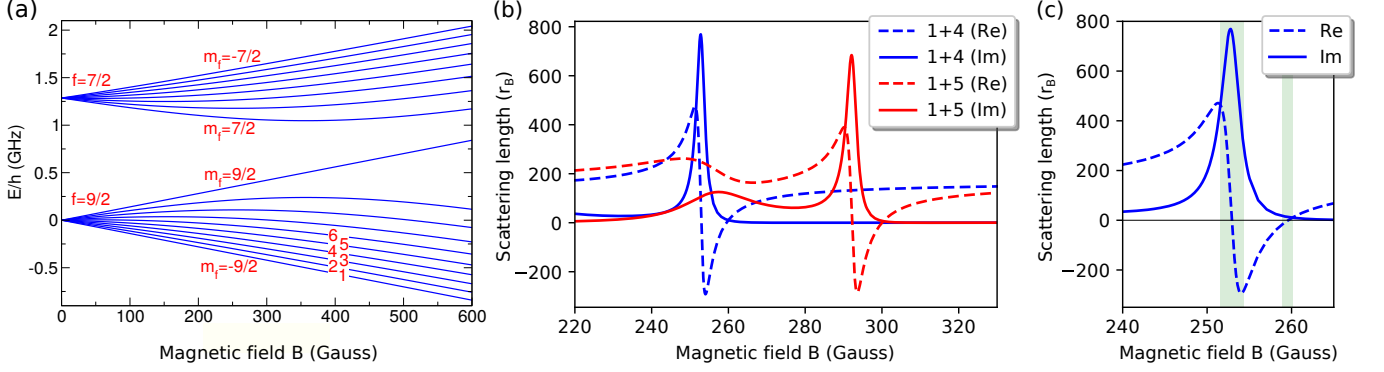


FIG. 3. **Magnetic Feshbach resonance for  $^{40}\text{K}$  atoms.** (a) The hyperfine-Zeeman energy levels  $E/h$  (GHz) of the  $f = 9/2$  and  $7/2$  manifolds versus magnetic field  $B$  (Gauss), labeled 1, 2, ... in order of increasing energy. The levels labeled 1, 2, ... have spin projections  $m_f = -9/2, -7/2, \dots$ , respectively. The spin and Zeeman coupling parameters are taken from Ref. [73]. (b) Scattering lengths of two  $^{40}\text{K}$  atoms. The solid and dashed lines represent  $\text{Im}(\tilde{a}_0)$  and  $\text{Re}(\tilde{a}_0)$ , respectively; blue and red represent the  $1 + 4$  and  $1 + 5$  channels, respectively. (c) Zoomed-in magnetic Feshbach resonance for the  $1 + 4$  channel. The shaded regions depict magnetic fields where the elastic interaction between two atoms is smaller than the pair loss rate, marking the regime of dissipative fermionic dynamics. All lengths are provided in Bohr-radius units  $r_B = 5.29 \cdot 10^{-9}$  cm, and the collision energy is  $E/k_B = 1\mu\text{K}$ , where  $k_B$  is the Boltzmann constant.

### A. Feshbach resonance

The Feshbach resonance provides a perfect tool to manipulate interactions between trapped atoms. Several mechanisms are available for practical use including magnetic, optical, and orbital Feshbach resonance [32, 35, 36]. For concreteness, we only study magnetic resonance here. The other two mechanisms have a qualitatively similar effect on atomic interactions. We study magnetic Feshbach resonance since it does not involve laser transitions and potentially has smaller scope for error.

We also require a fermionic atom that can be cooled, trapped and prepared in specific spin states with the requisite interaction properties. A promising example we illustrate here is the  $^{40}\text{K}$  atom in its  $^2\text{S}$  atomic ground state, which has an electron spin  $S = 1/2$  and nuclear spin  $I = 4$ , giving rise to total spin  $f = 9/2$  or  $7/2$ . The Zeeman substructure of the ground-state hyperfine manifold, shown in Fig. 3(a), gives rise to magnetically tunable Feshbach resonances in the interaction of two atoms for controlling elastic and dissipative collisions [35, 36].

It is straightforward to set up and numerically solve for the scattering and bound states of two  $^{40}\text{K}$  atoms, including the atomic electrons and nuclear spins, their mutual interactions, and the mass-scaled adiabatic Born-Oppenheimer molecular potentials for the  $^1\Sigma_g^+$  and  $^3\Sigma_u^+$  states [74]. We use the standard coupled channels method [35, 75] to set up the full spin Hamiltonian and solve the matrix Schrödinger equation for the scattering states. Such models, when calibrated against bound state and scattering data, provide highly accurate predictions of the properties associated with magnetically tunable Feshbach resonance states used to tune the scattering properties of two ultracold K atoms [74, 76–82].

The collision of two  $^{40}\text{K}$  atoms is characterized by the quantum numbers of the two separated atoms with resultant total spin projection  $m_F = m_{f1} + m_{f2}$  and relative angu-

lar momentum, or “partial wave,”  $\ell$  and  $M_\ell$ . States with the same total angular momentum  $M_{tot}$  are coupled in the molecular Hamiltonian for two atoms. Two like fermions collide with odd partial waves, e.g., the  $p$ -wave with  $\ell = 1$ , whereas two unlike fermions can collide via even or odd partial waves, including the  $s$ -wave with  $\ell = 0$ . A collision “channel” is defined by the partial wave and the spin quantum numbers of the two atoms. Strong pair loss via spin-exchange interactions is only possible if there is a product channel available with the same  $M_{tot}$  and  $\ell$  as the entrance channel; otherwise weak spin-dipolar spin relaxation is possible where  $m_F$  and  $m_\ell$  change by 2 units, conserving  $M_{tot}$ . Strong  $s$ -wave spin-exchange relaxation is possible for the spin channels  $1 + 4$  or  $1 + 5$ , but not for  $1 + 2$  or  $1 + 3$  channels; furthermore, only weak  $s$ -wave spin-dipolar spin relaxation is possible in the  $1 + 3$  channel. We also will not consider the much weaker  $p$ -wave spin-relaxation in these channels at ultracold temperatures (see below). Consequently, we now concentrate on the  $1 + 4$  and  $1 + 5$   $s$ -wave collisions for engineering dissipative collisions with weak on-site unitary interaction.

Very-low-energy  $s$ -wave elastic and dissipative collisions in the threshold regime are adequately described by a complex scattering length  $\tilde{a}_0$  [83, 84], defined as the  $k \rightarrow 0$  limit of the energy-dependent complex scattering length [85–88],

$$\tilde{a}_k = \frac{1}{ik} \frac{1 - S(k)}{1 + S(k)}. \quad (32)$$

Here  $\hbar k$  is the relative collisional momentum for a collision of two atoms with reduced mass  $\mu$  at energy  $E = \hbar^2 k^2 / (2\mu)$ , and  $S(k)$  is the diagonal element of the unitary  $S$ -matrix for the collision channel in question. In this subsection, we keep track of  $\hbar$  for added clarity. The coupling constant for the low-energy zero-range regularized pseudopotential approximation for atomic interactions is  $g = 2\pi\hbar^2 \text{Re}(\tilde{a}_0) / \mu$  [35, 36, 89]. The dissipative loss rate  $\dot{n}_1 = \dot{n}_2 = -K_2 n_1 n_2$  from colliding atoms in a gas with densities  $n_1$  and  $n_2$  is given by the



rate constant  $K_2 = -4\pi\hbar \text{Im}(\tilde{a}_0)/\mu$  [85, 86] (since  $\text{Im}(\tilde{a}_0)$  is zero or negative,  $K_2$  is positive definite;  $g$  can be positive or negative).

Using counterpropagating laser beams, it is possible to construct an array of trapping cells in an optical lattice structure [90]. Each cell is approximately harmonic and, in its ground state, may hold exactly zero, one, or two atoms. The scattering length formulation can readily be adapted to two atoms in an optical lattice cell to calculate the interaction energy or dissipative loss rate. For a harmonic trap with frequency  $\nu = \omega/(2\pi)$ , the analytic interaction energy for the lattice ground state from the zero-range pseudopotential is  $(3/2 + (2/\sqrt{\pi}) \text{Re}(\tilde{a}_0)/d)\hbar\omega$ , where the harmonic length  $d = \sqrt{\hbar/(\mu\omega)}$  [91]. If the lattice zero point energy  $3\hbar\omega/2$  is large enough,  $\text{Re}(\tilde{a}_k)$  may need to be evaluated at the lattice eigenenergy instead of taking  $\text{Re}(\tilde{a}_0)$  in the  $k \rightarrow 0$  limit [92, 93]. The decay rate  $\Gamma$  of an atom from the cell is given by  $K_2\bar{n}$ , where  $\bar{n} = \int d\mathbf{r} |\Psi_0(\mathbf{r})|^4 = 1/(\pi^{3/2}d^3)$  can be interpreted as a mean local density in the ground state of the lattice cell with wave function  $\Psi_0(\mathbf{r})$  [94].

The figure of merit for our dissipative quantum gate, the opposite requirement from that of Ref. [94], is that  $|\text{Im}(\tilde{a}_0)/\text{Re}(\tilde{a}_0)| \gg 1$ . This is possible to achieve using two  $^{40}\text{K}$  atoms in states 1 and 4 or states 1 and 5, as we now show from our coupled channels calculations. Using the mass scaled potentials of Ref. [74] and including  $s$ - and  $d$ -waves ( $\ell = 0$  and 2) in the coupled channels expansion for unlike spin species gives the scattering lengths shown in Fig. 3(b).

There are two regimes where the interaction energy proportional to  $\text{Re}(\tilde{a}_0)$  is small and the dissipation rate proportional to  $\text{Im}(\tilde{a}_0)$  is large. These are in the “core” of the resonance, rounded into a dispersive shape by the decay, and near the zero crossing where  $\text{Re}(\tilde{a}_0) = 0$ .

In order to get a sense of time scales, we can assume a harmonic length on the order of 100nm, for which  $\bar{n} \approx 2 \times 10^{14} \text{ cm}^{-3}$ . If we take the van der Waals length  $R_{\text{vdW}}$  of two  $^{40}\text{K}$  atoms, 3.4nm [35], as a “typical” size for  $\text{Im}(\tilde{a}_0)$ , then  $K_2 \approx 1.3 \times 10^{-10} \text{ cm}^3/\text{s}$ , giving a decay time of  $\Gamma^{-1} = 40 \mu\text{s}$ . The next subsection discusses how such magnitudes could enable the realization of dissipation-assisted quantum computing.

We note that there are other spin channels for  $^{40}\text{K}$  and in other species where Feshbach tuning of a favorable ratio  $\text{Im}(\tilde{a}_k/d)/\text{Re}(\tilde{a}_k/d) \gg 1$  could be feasible. This may be possible for like fermions, where only  $p$ -wave channels are available. However,  $p$ -wave interactions, treated by Eq. (32) with a  $p$ -wave  $S$ -matrix element, are typically suppressed by a factor on the order of  $k^2 R_{\text{vdW}}^2$  relative to the range of  $s$ -wave processes, due to the threshold law for  $p$ -waves [86, 95–97]. This suppression factor is on the order of 0.001 for  $^{40}\text{K}$  atoms with an energy on the order of 1  $\mu\text{K}$ , so it would be harder to find ranges suitable for experimental control.

## B. Dissipation-assisted quantum computing

We now modify the idea from Sec. III to make it feasible for cold atomic systems. We limit our attention to two

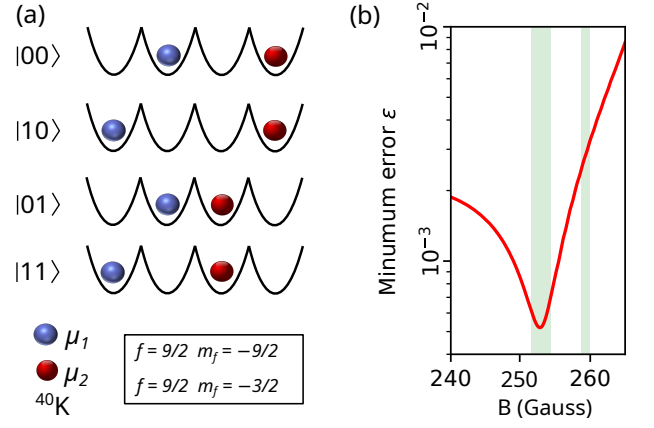


FIG. 4. **Dissipative gate utilizing cold atoms.** (a) Two-qubit logical states encoded using a pair of atoms in distinct states occupying four neighboring sites. (b) The upper bound for the total dissipative gate error as a function of magnetic field for  $^{40}\text{K}$ , given the background error rate  $\Gamma = 10^{-2} \text{ s}^{-1}$ . The shaded areas describe the weak interactions regime shown in Fig. 3(c).

distinct states of trapped atoms, denoted here as  $\mu_1$  and  $\mu_2$ . A single trap is described using the following four basis states: the empty state  $|0\rangle_i$ , single-occupied states  $|\mu_\alpha\rangle_i = c_{i\mu_\alpha}^\dagger |0\rangle_i$ ,  $\alpha = 1, 2$ , and the double-occupied state  $|\mu_1\mu_2\rangle_i = -|\mu_2\mu_1\rangle_i = c_{i\mu_1}^\dagger c_{i\mu_2}^\dagger |0\rangle_i$ . We consider the lattice Hamiltonian  $H = H_{\mu_1} + H_{\mu_2} + V$ , where  $H_\mu = \sum_{\langle ij \rangle} J_{ij}^\mu(t) (c_{i\mu}^\dagger c_{j\mu} + \text{h.c.}) + \sum_i \Delta_i^\mu(t) c_{i\mu}^\dagger c_{i\mu}$ . The quantities  $J_{ij}^\mu(t)$  are real tunneling amplitudes, and  $\Delta_i^\mu(t)$  are on-site potentials, both of which can depend on the atomic state  $\mu$ . Two distinct atoms located in the same trap are subject to elastic interactions  $V = E \sum_i n_{i\mu_1} n_{i\mu_2}$ , where  $E$  is the interaction energy and  $n_{i\mu} = c_{i\mu}^\dagger c_{i\mu}$  is the  $\mu$ -occupation number of the  $i$ th trap. As shown in Sec. IV A, the interaction  $E$  may be made to vanish for a specific pair of states  $\mu_1$  and  $\mu_2$  by, for example, manipulating the magnetic field as shown in Fig. 3(c). Also, atoms in the same trap undergo pair loss with rate  $\Gamma$ , described by Lindblad operators  $A_i = \Gamma c_{i\mu_1} c_{i\mu_2}$ . For  $E = 0$ , the entire dynamics is described by the master equation Eq. (1).

The computational scheme utilizes pairs of sites to encode individual logical qubits. The logical qubit states are  $|0\rangle_L = |0\rangle_{\mu_j}$  and  $|1\rangle_L = |\mu_j\rangle|0\rangle$ , irrespective of the atom’s type  $\mu_j$ . Single-qubit gates can be performed using the local potentials and coherent hopping between logical qubit sites. At the same time, we consider two distinct ways of constructing entangling gates, depending on the atomic electronic structure. The first method we consider is designed for alkaline-earth(-like) atoms such as  $^{87}\text{Sr}$  [31] and  $^{173}\text{Yb}$  [29, 30]. We can use nuclear-spin polarized metastable states  $^1S_0$  and  $^3P_0$  as the two species  $\mu_1$  and  $\mu_2$  [23] in order to apply a species-dependent hopping term  $J_{ij}^\mu$ . The scattering length between  $\mu_1$  and  $\mu_2$  can then be potentially tuned by optical or orbital Feshbach resonances to be purely imaginary. Alternatively, one could use  $^3P_2$  instead of  $^3P_0$ , in which case a magnetic Feshbach resonance is also an option. However, this method has limited applicability to alkali atoms, for ex-

ample  $^{87}\text{Rb}$  [24] or  $^{40}\text{K}$  (described above), where the states  $\mu_i$  are encoded into different angular momentum projections  $m_f$ . This is because a state-dependent lattice in alkali atoms [25] can exhibit significant single-atom dissipation rates. For alkali atoms, therefore, we propose an additional scheme that does not rely on an internal-state-dependent lattice and uses the same lattice potential for both states. In order to implement entangling gates, we will make use of single-qubit rotations with single-site resolution. This can be achieved using two-photon Raman transitions induced by focused laser beams or other similar techniques [26, 98, 99]. Both schemes can be used interchangeably.

We now give details of the two schemes. Consider the four two-qubit logical states  $|00\rangle_L = |0, \mu_1, 0, \mu_2\rangle$ ,  $|01\rangle_L = |0, \mu_1, \mu_2, 0\rangle$ ,  $|10\rangle_L = |\mu_1, 0, 0, \mu_2\rangle$ , and  $|11\rangle_L = |\mu_1, 0, \mu_2, 0\rangle$  [see Fig. 4(a)], where the comma separates states of individual traps. For the first scheme, an entangling control-Z gate is performed in a single step by applying the hopping  $H = J(c_{2\mu_2}^\dagger c_{3\mu_2} + \text{h.c.})$  for state  $\mu_2$  between traps 2 and 3 for time  $t = \pi/J$ . As a result, the states  $|00\rangle_L$  and  $|01\rangle_L$  remain invariant under the evolution, while any transitions involving the state  $|01\rangle_L$  are blocked by the quantum Zeno effect. In the limit  $\Gamma/J \rightarrow \infty$ , the overall unitary operation in the logical Hilbert space is described by the control-Z gate in Eq. (31). For the second scheme, the control-Z gate can be applied in three steps: (1) apply the state-independent hopping  $H = J\sum_i (c_{2\mu_i}^\dagger c_{3\mu_i} + \text{h.c.})$  between traps 2 and 3 for time  $t = \pi/(2J)$ ; (2) apply a single-qubit phase-gate  $|\mu_1\rangle_3 \rightarrow e^{i\pi}|\mu_1\rangle_3$ ,  $|\mu_2\rangle_3 \rightarrow |\mu_2\rangle_3$  on site 3; (3) repeat the first step. As a result, states  $|01\rangle_L$  and  $|10\rangle_L$  remain stationary, state  $|00\rangle_L$  acquires a total phase  $2\pi$  (from the phase gate and hopping), and state  $|11\rangle_L$  acquires phase  $\pi$ . Thus, the second scheme also implements a control-Z gate.

The performance of the gate can be disrupted by errors, including imperfect Zeno-effect error, the single-qubit phase gate error (for the second scheme), and background dissipation error. The background dissipation error can be bounded above by  $\Gamma't$ , where  $\Gamma'$  is the background dissipation rate, and  $t = \pi/J$  is the gate performance time (neglecting the time taken for the single-qubit phase gate). The single-qubit phase gate error  $\epsilon_0$  is fundamentally limited by light scattering loss during the Raman transition, which depends on the characteristic linewidth  $\gamma$  of the excited levels and the detuning limited by fine structure splitting  $\Delta$ . This error is estimated to be  $\epsilon_0 \sim \gamma/\Delta$ . Deviations from perfect single-site addressability during the single-qubit phase gate can also give rise to errors, which can nevertheless be greatly reduced by subwavelength addressability techniques [25, 26, 99–103]. Finally, the error caused by an imperfect Zeno effect can be approximated by the first term in the Taylor expansion of the infidelity in  $(\Gamma t)^{-1}$  (see Appendix E), leading to the total error

$$\epsilon = \epsilon_0 + \Gamma't + \frac{8\pi^2}{\Gamma t} \frac{1}{1 + 4\zeta^2} + O\left(\frac{1}{\Gamma^2 t^2}\right), \quad (33)$$

where  $\zeta = E/\Gamma$  is the loss-to-interaction ratio. The error can be minimized by making the choice  $t = 2\pi/\sqrt{\Gamma\Gamma'(1 + 4\zeta^2)}$ ,

leading to the expression

$$\epsilon = \epsilon_0 + 4\pi\sqrt{\frac{\Gamma'}{\Gamma(1 + 4\zeta^2)}}. \quad (34)$$

The dependence of the second term on the magnetic field is illustrated in Fig. 4(b) under the same choice of parameters as in Fig. 3. For a suitable choice of magnetic field strength, the theoretical upper bound for the error can be as low as  $\epsilon \sim 5 \cdot 10^{-4}$  for the background dissipation rate  $\Gamma' = 10^{-2}\text{s}^{-1}$ . For  $^{40}\text{K}$  atoms, the optical transition error  $\epsilon_0$  can be estimated using the values  $\gamma \simeq 2\pi \times 6.0\text{ MHz}$  and  $\Delta \simeq 2\pi \times 1.7\text{ THz}$  [104], leading to the upper bound  $\epsilon_0 \sim 10^{-6}$ , which is an insignificant contribution to the overall error. As a result, the theoretical bound for the gate error approaches the characteristic thresholds given by many error-correcting schemes.

## V. DISCUSSION

In this work, we have demonstrated how simple forms of dissipation affect the complexity of simulation of noninteracting fermions. In particular, focusing on linear-quadratic Lindblad operators, we have shown the existence of two complementary complexity classes of Lindblad operators, easy and hard for simulation on a classical computer. Using the error-correction formalism, we showed that the hard class has a finite volume in the parameter space and tolerates the presence of small arbitrary corrections. At the same time, the easy classes may have small measure and could become hard even as a result of arbitrarily small corrections to the master equation.

We have expanded the region of classical simulability of free-fermions in the presence of Markovian errors from single-qubit loss/gain to more general quadratic-linear Lindblad operators. The algorithms we devise for EC1–EC3 based on the stochastic unraveling approach provably work in polynomial time. This shows that a large class of dissipation processes such as dephasing or single-fermion decay can be treated with the help of efficient classical algorithms.

At the same time, more complex processes are BQP-complete, which we show by explicitly constructing an entangling gate and showing the equivalence of the problem with universal quantum computation. We thus place limitations on the extent to which the simulability result may be extended, since we believe quantum computation is strictly more powerful than classical computation. Our detailed analysis shows that it is within the range of experimental feasibility to implement with cold atoms a quantum computer with purely dissipative atom-atom interactions, an exciting possibility for experiments in quantum computing. For example, dissipative quantum systems such as alkaline-earth atoms may serve in the next generation of quantum supremacy experiments. Also, our result suggests that simulating fermion dynamics may be hard for quantum particles experiencing dissipation, for example, quasiparticles in solid-state systems. Future work can explore the hardness of simulation of electronic systems

with quasiparticle dynamics approximated with quadratic-linear Lindblad operators that include the effects of electron-electron, electron-phonon, and electron-impurity scattering processes. Alternatively, physical systems following such dynamics with high accuracy may be a future platform for quantum computing experiments.

It may be interesting to explore the connection of our results with the theory of matchgate (free-fermion) computations and the role played by non-Gaussianity. Quadratic fermionic Hamiltonians and single-fermion loss give rise to Gaussian operations and are hence easily simulable [17]. It is known [105] that any non-Gaussian fermionic state is a resource for fermionic computation, boosting the computational power of free fermions from being classically simulable to being universal for quantum computation. Our results suggest that quadratic-linear Lindblad operators are non-Gaussian in general. Therefore, it would be interesting to quantify the amount of non-Gaussianity (or “magic”) for the Lindblad operations we study here.

Further, one may also consider how the complexity of simulating dynamics under quadratic Lindbladians changes with time. Since the system starts off in a Fock state that is easy to sample from, and dynamics under quadratic Hamiltonians with quadratic Lindbladians can generate states that are hard to sample from, one can see a dynamical transition in sampling complexity [13, 106]. This gives rise to interesting questions in Lieb-Robinson-like bounds for the time-evolution of free particles in the presence of noise. The study of worst-to-average-case equivalence in complexity, which seeks to understand the complexity of typical instances as opposed to worst-case instances, is also an exciting direction [68, 107]. It is an open question whether the Cayley path technique of Ref. [107] can be adapted to argue for average-case hardness of dissipative fermionic dynamics.

## ACKNOWLEDGMENTS

We thank Bill Fefferman, Mohammad Hafezi, Trey Porto, and Daniel Gottesman for fruitful discussions. This work was supported by DoE ASCR FAR-QC (award No. DE-SC0020312), DoE BES Materials and Chemical Sciences Research for Quantum Information Science program (award No. DE-SC0019449), NSF PFCQC program, DoE ASCR Quantum Testbed Pathfinder program (award No. DE-SC0019040), AFOSR, ARO MURI, ARL CDQI, and NSF PFC at JQI.

## Appendix A: Easy Class 1

In this appendix section, we analyze the convergence of the average unitary stochastic evolution to the exact Lindblad dynamics in the case of Easy Class 1 (EC1). First, we set the initial time to be zero and consider the final time  $t$  being an integer multiple of timestep  $\Delta\tau$ . This assumption holds without loss of generality since  $\Delta\tau$  may be adjusted appropriately to capture any particular final time. Then the overall evolution

of unitary can be written as a product

$$U(t) = \prod_{n=0}^{t/\Delta\tau} U_n, \quad (\text{A1})$$

where the timestep unitary  $U_n$  is expressed in terms of a time-ordered exponential

$$U_n = \mathcal{T} \exp\left(-i \int_{n\Delta\tau}^{(n+1)\Delta\tau} dt H'(t)\right) \quad (\text{A2})$$

generated by the stochastic Hamiltonian  $H'(t)$  in Eq. (13),

$$H'(t) = H(t) + \frac{R(t)}{\sqrt{\Delta\tau}}. \quad (\text{A3})$$

Here  $H(t)$  is the original time-dependent Hamiltonian, and  $R(t) = \sum_k \xi_{nk} A_k(t) + \xi_{nk}^* A_k^\dagger(t)$  is the normalized stochastic part, where  $\xi_{nk}$  are independent complex Gaussian variables defined for times  $n\Delta\tau \leq t \leq (n+1)\Delta\tau$ .

Let us consider the ordered exponential expansion of the timestep unitary in Eq. (A2):

$$\begin{aligned} U_n = I &- i\Delta\tau^{1/2} R_n - \Delta\tau \left( iH_n + \frac{1}{2} R_n^2 \right) \\ &- \Delta\tau^{3/2} \left( \mathcal{P} H_n R_n - \frac{i}{6} R_n^3 \right) \\ &- \frac{1}{2} \Delta\tau^2 \left( H_n^2 - \frac{i}{3} \mathcal{P} H_n R_n R_n - \frac{1}{12} R_n^4 \right) \\ &+ O(\Delta\tau^{5/2}), \end{aligned} \quad (\text{A4})$$

where we denote the discretized value of an operator  $O_n$  and permutation sum respectively as

$$\begin{aligned} O_n &= \frac{1}{\Delta\tau} \int_n dt O(t) \equiv \frac{1}{\Delta\tau} \int_{n\Delta\tau}^{(n+1)\Delta\tau} dt O(t), \\ \mathcal{P} O_1 \dots O_m &= \sum_{\sigma \in S_m} O_{\sigma(1)} \dots O_{\sigma(m)}. \end{aligned} \quad (\text{A5})$$

The average over the stochastic field can be taken for each timestep independently. Therefore, the effect of the timestep unitary in Eq. (A4) is

$$\begin{aligned} \mathbb{E} U_n \rho U_n^\dagger &= \left( I + \mathcal{L}_n \Delta\tau + \frac{1}{2} \mathcal{L}_n^2 \Delta\tau^2 \right) \rho \\ &+ \mathcal{D}_n \rho \Delta\tau^2 + O(\Delta\tau^3). \end{aligned} \quad (\text{A6})$$

In the equation above,  $\mathcal{L}_n$  is the generator of the original Lindblad equation,  $\lim_{\Delta\tau \rightarrow 0} \mathcal{L}_n = \mathcal{L}(n\Delta\tau)$ , expressed as

$$\begin{aligned} \mathcal{L}_n \rho &= -i[H_n, \rho] + \sum_k \left( A_{kn} \rho A_{kn}^\dagger - \frac{1}{2} \{A_{kn}^\dagger A_{kn}, \rho\} \right) \\ &+ \sum_k \left( A_{kn}^\dagger \rho A_{kn} - \frac{1}{2} \{A_{kn} A_{kn}^\dagger, \rho\} \right), \end{aligned} \quad (\text{A7})$$

and  $\mathcal{D}_n$  represents the lowest-order correction occurring due to the timestep being nonzero:

$$\begin{aligned} \mathcal{D}_n \rho = & \frac{1}{4} \sum_{kk'} \left( A_{k'n}^\dagger A_{kn}^\dagger \rho [A_{k'n}, A_k] + A_{k'n}^\dagger A_{kn} \rho [A_{k'n}, A_{kn}^\dagger] \right. \\ & \left. + A_{k'n} A_{kn}^\dagger \rho [A_{k'n}, A_k] + A_{k'n} A_{kn} \rho [A_{k'n}, A_{kn}^\dagger] \right) \\ & + \sum_k \left( A_{kn} \rho V_{kn} + V_{kn} \rho A_{kn} + V_{kn}^\dagger \rho A_{kn}^\dagger + A_{kn}^\dagger \rho V_{kn}^\dagger \right) \\ & + W_n \rho + \rho W_n^\dagger. \end{aligned} \quad (\text{A8})$$

Here we have used the notation

$$\begin{aligned} V_{kn} &= \sum_{k'} \frac{1}{4} \{ A_{kn}^\dagger, \{ A_{k'n}^\dagger, A_{k'n} \} \} - \frac{1}{6} \mathcal{P} A_{kn}^\dagger A_{k'n}^\dagger A_{k'n}, \\ W_n &= -\frac{i}{6} \sum_k \left( [ [H_n, A_{kn}], A_{kn}^\dagger ] + \{ H_n, A_{kn}^\dagger A_{kn} \} \right) \\ &\quad - \frac{1}{8} \left( \sum_k \{ A_{kn}^\dagger, A_{kn} \} \right)^2 + \frac{1}{48} \sum_{kk'} \mathcal{P} A_{kn}^\dagger A_{kn} A_{k'n}^\dagger A_{k'n}. \end{aligned} \quad (\text{A9})$$

The overall expression in Eq. (A8) can be written in a compact form,

$$\mathcal{D}_n \rho = \sum_{\alpha} D_{\alpha n}^{(1)} \rho D_{\alpha n}^{(2)}, \quad (\text{A10})$$

where  $D_{\alpha n}^{(i)} = \text{poly}(H_n, A_{kn})$  are polynomials of degree less than four.

The averaged stochastic map in Eq. (A6) can be rewritten as a continuous evolution and then decomposed using Dyson series for the small parameter  $\Delta\tau$ ,

$$\begin{aligned} \mathbb{E} \mathcal{V}_{\text{st}}(t_2, t_1) &= \mathcal{T} \exp \left( \int_{t_1}^{t_2} dt' (\mathcal{L}(t') + \mathcal{D}(t') \Delta\tau) \right) + O(\Delta\tau^2) \\ &= \mathcal{V}(t_2, t_1) + \int_{t_1}^{t_2} dt' \mathcal{V}(t_2, t') \mathcal{D}(t') \mathcal{V}(t', t_1) \Delta\tau + O(\Delta\tau^2), \end{aligned} \quad (\text{A11})$$

where the generators  $\mathcal{L}(t)$  and  $\mathcal{D}(t)$  are continuous versions of the operators in Eq. (A7) and Eq. (A8), in which the  $\Delta\tau$ -averaged operators  $A_{kn}$  and  $H_n$  are replaced by the corresponding instantaneous values at time  $t$ , i.e.  $A(t)$  and  $H(t)$ , respectively. To obtain the expression in Eq. (17), we recursively replace  $\mathcal{V}(t_2, t')$  and  $\mathcal{V}(t', t_1)$  on the right-hand side by their stochastic average and collect all  $O(\Delta\tau^2)$  terms.

## Appendix B: Easy Class 2

In this appendix section, we analyze the convergence of the average stochastic unitary evolution to the Lindblad dynamics in the case of Easy Class 2 (EC2). The single timestep evolution averaged over stochastic unitaries in Eq. (19) is equivalent

to the map

$$\begin{aligned} \mathbb{E} U_n \rho U_n^\dagger &= U_n^0 \left( \rho + \int_n dt \sum_k \Gamma_k(t) (Y_k(t) \rho Y_k^\dagger(t) - \rho) \right) U_n^{0\dagger} \\ &= \left( I + \mathcal{L}_n + \frac{1}{2} \mathcal{L}_n^2 \right) \rho + \mathcal{D}_n \rho \Delta\tau^2 + O(\Delta\tau^3), \end{aligned} \quad (\text{B1})$$

where the target Liouville operator is

$$\mathcal{L}_n \rho = -i[H_n, \rho] + \sum_k A_{kn} \rho A_{kn}^\dagger - \Gamma_{kn} \rho. \quad (\text{B2})$$

The correction now takes the form

$$\begin{aligned} \mathcal{D}_n \rho &= \sum_k \left( A_{kn} \rho C_{kn} + C_{kn}^\dagger \rho A_{kn}^\dagger \right) \\ &\quad - \frac{1}{2} \sum_{kk'} A_{kn} A_{k'n} \rho A_{k'n}^\dagger A_{kn}^\dagger - \frac{1}{2} \Gamma_n^2 \rho, \end{aligned} \quad (\text{B3})$$

denoting  $C_{kn} = \Gamma_n A_{kn}^\dagger + \frac{i}{2} [A_{kn}^\dagger, H_n]$  and  $\Gamma_n = \Delta\tau^{-1} \int_n dt \sum_k \Gamma_k(t)$ . This expression has the form of Eq. (A10) with operators  $D_{\alpha n}^{(i)}$  being a sum of products of at most four Majorana fermion operators.

## Appendix C: Easy Class 3

In this appendix section, we analyze Easy Class 3 (EC3) and show the convergence of the system-ancilla stochastic evolution under the Hamiltonian in Eq. (13) using the stochastic operators in Eq. (20) to the dissipative dynamics with linear Lindblad operators. Let us start from a many-body pure state of the fermions occupying  $L$  modes of the system and  $L_a$  ancilla modes at time  $t = n\Delta\tau$ , denoting it as  $|\Psi_n\rangle$ . At the  $n$ th timestep, the evolution acts on the system and the  $n$ th ancilla mode only. Thus, the state at time  $t = n\Delta\tau$  is a product state of subsystem states: (1) correlated state of  $L$  system modes together with the first  $n$  ancilla modes and (2) the product states of the remaining  $L_a - n$  ancilla modes, i.e.

$$|\Psi_n\rangle = |\phi_n\rangle_{L+n} \otimes |0\rangle_{L_a-n}. \quad (\text{C1})$$

The evolution is governed by the Hamiltonian

$$H'(t) = H(t) \otimes I_A + \frac{1}{\sqrt{\Delta\tau}} \left( K(t) + K^\dagger(t) \right), \quad (\text{C2})$$

where the stochastic terms are

$$K(t) = \sum_k f_{nk} A_k(t) (\gamma_{2(L+n-1)} + i\gamma_{2(L+n-1)}) \quad (\text{C3})$$

at times  $n\Delta\tau \leq t \leq (n+1)\Delta\tau$ , and  $f_{nk}$  are independent real Gaussian variables. Then, at the  $(n+1)$ th step, the system-



ancilla state  $|\Psi_n\rangle = U_n|\Psi_n\rangle$  is

$$\begin{aligned}
|\Psi_{n+1}\rangle &= |\Psi_n\rangle - i\Delta\tau^{1/2}K_n|\phi_n\rangle|1\rangle|0\rangle_{T-n-1} \\
&\quad - \Delta\tau\left(iH_n + \frac{1}{2}K_n^\dagger K_n\right)|\phi_n\rangle|0\rangle_{L_a-n} \\
&\quad - \Delta\tau^{3/2}\left(\frac{1}{2}\{H_n, K_n\} - \frac{i}{6}K_n K_n^\dagger K_n\right)|\phi_n\rangle|1\rangle|0\rangle_{L_a-n-1} \\
&\quad - \frac{1}{2}\Delta\tau^2\left(H_n^2 - \frac{i}{3}\{H_n, K_n^\dagger K_n\} \right. \\
&\quad \quad \left. - \frac{i}{3}R_n^\dagger H_n K_n - \frac{1}{12}(K_n^\dagger K_n)^2\right)|\phi_n\rangle|0\rangle_{L_a-n} \\
&\quad + O(\Delta\tau^{5/2}),
\end{aligned} \tag{C4}$$

where we used the discrete-time operator values  $H_n$  and  $K_n$  obtained as in Eq. (A4).

The interpolated continuous-time evolution for the density matrix of the system can be presented in the form

$$\begin{aligned}
\frac{d}{dt}\rho &= \frac{1}{\Delta\tau}\mathbb{E}\text{Tr}_A\left(|\Psi_{n+1}\rangle\langle\Psi_{n+1}| - |\Psi_n\rangle\langle\Psi_n|\right)\Big|_{n=\lfloor t/\Delta\tau\rfloor} \\
&= \left(I + \mathcal{L}_n + \frac{1}{2}\mathcal{L}_n^2\right)\rho + \mathcal{D}_n\rho\Delta\tau^2 + O(\Delta\tau^3),
\end{aligned} \tag{C5}$$

where  $\lfloor x \rfloor$  is the floor function. The target Liouville operator is

$$\mathcal{L}_n\rho = -i[H_n, \rho] + \sum_k A_{kn}\rho A_{kn}^\dagger - \frac{1}{2}\{A_{kn}^\dagger A_{kn}, \rho\} \tag{C6}$$

and the correction is

$$\begin{aligned}
\mathcal{D}_n\rho &= \sum_{kk'}\left(\frac{1}{4}A_k^\dagger A_{k'}\rho A_{k'}^\dagger A_k - \frac{1}{2}A_k A_{k'}\rho A_{k'}^\dagger A_k^\dagger\right) \\
&\quad + \sum_k\left(A_k\rho Q_k + Q_k^\dagger\rho A_k^\dagger\right) + M\rho + \rho M^\dagger,
\end{aligned} \tag{C7}$$

where

$$\begin{aligned}
Q_k &= \frac{1}{12}\{A_k^\dagger, A_{k'}^\dagger A_{k'}\} \\
M &= \frac{i}{6}\sum_k\left(A_k^\dagger H A_k - \frac{1}{2}\{H, A_k^\dagger A_k\}\right) \\
&\quad - \frac{1}{12}\sum_{kk'}\left(A_{k'}^\dagger A_{k'} A_k^\dagger A_k - \frac{1}{2}A_{k'}^\dagger A_k A_k^\dagger A_{k'}\right).
\end{aligned} \tag{C8}$$

As is the case for EC1 and EC2, the correction is described by Eq. (A10) with operators  $D_{\alpha n}^{(i)}$  being a sum of products of at most eight Majorana fermion operators.

## Appendix D: Error analysis

In this appendix section, we first derive Eq. (22) and then provide the proof of the Lemma in the main text.

The error can be formally expressed in terms of evolution superoperators as

$$\epsilon = \frac{1}{2}\max_{\mathbf{r}'}\sum_{\mathbf{r}}|\langle\mathbf{r}|\mathbb{E}\mathcal{V}_{\text{st}}(t, 0)\rho_{\mathbf{r}'}(0) - \mathcal{V}(t, 0)\rho_{\mathbf{r}'}(0)|\mathbf{r}\rangle|, \tag{D1}$$

where  $\mathcal{V}(t_2, t_1)$  is the Markovian map generated by Eq. (1) in the main text,  $\mathcal{V}_{\text{st}}(\xi, t_2, t_1)$  is a unitary trajectory map depending on either a realization of the discrete stochastic field  $\xi_{kn}$  (EC1 and EC3) or a random choice of unitaries (EC2). We use the Dyson-like expansion in Eq. (17) and the convexity of the absolute value to upper bound the error as

$$\begin{aligned}
\epsilon &\leq \frac{\Delta\tau}{2}\mathbb{E}\max_{\mathbf{r}'}\int_0^t dt' \sum_{\mathbf{r}}|\langle\mathbf{r}|\mathcal{V}_{\text{st}}(t, t')\mathcal{D}(t')\mathcal{V}_{\text{st}}(t', 0)\rho_{\mathbf{r}'}|\mathbf{r}\rangle| \\
&\quad + O(\Delta\tau^2).
\end{aligned} \tag{D2}$$

Using the fact that  $\mathcal{V}_{\text{st}}$  is a unitary map, we can rewrite

$$\mathcal{V}_{\text{st}}(t', 0) = \mathcal{V}_{\text{st}}^{-1}(t', t)\mathcal{V}_{\text{st}}(t, 0), \tag{D3}$$

where the inverse of a unitary map is well-defined through the inverse unitary transformations. This expression leads directly to Eq. (22), taking into account that

$$\mathcal{V}_{\text{st}}^{-1}(t', t)\mathcal{D}(t)\rho\mathcal{V}_{\text{st}}^{-1}(t', t) = \sum_{\alpha} D_{\alpha}^{(1)}(t, t')\rho D_{\alpha}^{(2)}(t, t'), \tag{D4}$$

where  $D_{\alpha}^{(i)}(t, t') = \mathcal{V}_{\text{st}}(t, t')D_{\alpha}^{(i)}(t')$ .

### 1. Proof of the Lemma

Let us rewrite the left-hand side of Eq. (25) using the spectral decomposition  $\rho = \sum_{\mu} p_{\mu}|\psi_{\mu}\rangle\langle\psi_{\mu}|$  and triangle inequality as

$$\begin{aligned}
\sum_{\mathbf{r}}|\langle\mathbf{r}|O_1\rho O_2|\mathbf{r}\rangle| &= \sum_{\mathbf{r}}\left|\sum_{\mu, \mathbf{r}_1, \mathbf{r}_2} p_{\mu}\psi_{\mathbf{r}_1}^{\mu}\psi_{\mathbf{r}_2}^{\mu*}\langle\mathbf{r}|O|\mathbf{r}_1\rangle\langle\mathbf{r}_2|O|\mathbf{r}\rangle\right| \\
&\leq \sum_{\mu} p_{\mu}\sum_{\mathbf{r}}\sum_{\mathbf{r}_1, \mathbf{r}_2} |\psi_{\mathbf{r}_1}^{\mu}||\psi_{\mathbf{r}_2}^{\mu}||\langle\mathbf{r}|O|\mathbf{r}_1\rangle||\langle\mathbf{r}_2|O|\mathbf{r}\rangle| \\
&\leq \|O_1\|_{\max}\|O_2\|_{\max}\sum_{\mu, \mathbf{r}}\sum_{\mathbf{r}_1 \in D(k_1, \mathbf{r})}\sum_{\mathbf{r}_2 \in D(k_2, \mathbf{r})} p_{\mu}|\psi_{\mathbf{r}_1}^{\mu}||\psi_{\mathbf{r}_2}^{\mu}|,
\end{aligned} \tag{D5}$$

where we denote  $\|O\|_{\max} = \max_{ij}|O_{ij}|$  to be the max-norm of the matrix  $O$ , and  $D_k(\mathbf{r})$  is a sphere with radius  $k$  with respect to Hamming distance. Using the inequality

$$|\psi_{\mathbf{r}_1}^{\mu}||\psi_{\mathbf{r}_2}^{\mu}| \leq \frac{1}{2}\left(|\psi_{\mathbf{r}_1}^{\mu}|^2 + |\psi_{\mathbf{r}_2}^{\mu}|^2\right) \tag{D6}$$

and the property that the sphere  $D(k, \mathbf{r})$  contains  $\binom{L}{k} \leq L^k/k!$  states, we obtain

$$\sum_{\mathbf{r}}|\langle\mathbf{r}|O_1\rho O_2|\mathbf{r}\rangle| \leq \frac{1}{k_1!k_2!}\|O_1\|_{\max}\|O_2\|_{\max}L^{k_1+k_2}, \tag{D7}$$

where we use the fact that the density matrix is properly normalized,  $\text{Tr } \rho = 1$ .

### Appendix E: Dissipative gates errors

In this appendix section, we derive the error of dissipative gates analyzed in Sections III and IV.

In the case of imperfect Zeno blockade, the major source of error is associated with leakage to the out-of-logic states. In the scheme proposed in Section III, there are two relevant out-of-logic states into which leakage occurs from the state  $|00\rangle_L = |0101\rangle$ , namely  $|0011\rangle$  and  $|0000\rangle$ . The first of these states ( $|0011\rangle$ ) is accessed via a unitary channel, while the second of these states ( $|0000\rangle$ ) is accessed via a dissipative channel. The simplest way to describe leakage is to consider unitary evolution of basis states  $\{|0101\rangle, |0011\rangle\}$  and including the second-channel leakage using a non-Hermitian term. The resulting non-Hermitian Hamiltonian is

$$H_S = \begin{pmatrix} 0 & J \\ J & -\frac{i}{2}\Gamma \end{pmatrix}. \quad (\text{E1})$$

The leakage error can be computed as

$$|\langle 00|_L S |00\rangle_L|^2 \equiv 1 - 2\epsilon = 1 - \frac{4\pi}{\gamma} + O\left(\frac{1}{\gamma^2}\right), \quad (\text{E2})$$

where  $S = \exp(-i\pi H_S/J)$  and  $\gamma = \Gamma/J$ .

For the scheme involving cold atoms in Section IV, the rel-

evant out-of-logic states are

$$\begin{aligned} |P1\rangle &= |0, \mu_2\mu_1, 0, 0\rangle, \\ |P2\rangle &= |0, 0, \mu_1\mu_2, 0\rangle, \\ |EX\rangle &= |0, \mu_2, \mu_1, 0\rangle, \\ |VC\rangle &= |0, 0, 0, 0\rangle. \end{aligned} \quad (\text{E3})$$

The restriction of the effective Hamiltonian to the subspace spanned by the basis  $\{|01\rangle, |P1\rangle, |P2\rangle, |EX\rangle\}$  is

$$H'_S = \begin{pmatrix} 0 & J & J & 0 \\ J & E - \frac{i}{2}\Gamma & 0 & J \\ J & 0 & E - \frac{i}{2}\Gamma & J \\ 0 & J & J & 0 \end{pmatrix}, \quad (\text{E4})$$

where  $E$  is the interaction energy of a fermion pair on the same site. The non-Hermitian nature of the Hamiltonian reflects additional leakage to the fully empty state  $|VC\rangle$  due to pair loss. In the strong dissipation limit  $J \ll \Gamma$ , the leakage error  $\epsilon$  for the gate can be defined as

$$\begin{aligned} 1 - 2\epsilon &\equiv |\langle 01|_L S' |01\rangle_L|^2 \\ &= 1 - \frac{8\pi^2}{\Gamma t} \frac{1}{1 + 4\zeta^2} + O\left(\frac{1}{\Gamma^2 t^2}\right), \end{aligned} \quad (\text{E5})$$

where  $S' = \exp(-iH'_S t)$ ,  $t = \pi/J$  is the characteristic time of hopping between lattice sites, and  $\zeta = E/\Gamma$  is the ratio between the interaction energy and the pair loss rate.

- 
- [1] Michael A. Nielsen and Isaac L. Chuang, *Quantum Computation and Quantum Information: 10th Anniversary Edition* (Cambridge University Press, 2010).
  - [2] Richard P Feynman, "Simulating physics with computers," *Int. J. Theor. Phys* **21**, 467–488 (1982).
  - [3] Seth Lloyd, "Universal quantum simulators," *Science* **273**, 1073–1078 (1996).
  - [4] Emanuel Knill, "Fermionic linear optics and matchgates," [arXiv:quant-ph/0108033](https://arxiv.org/abs/quant-ph/0108033) (2001).
  - [5] Leslie G Valiant, "Quantum circuits that can be simulated classically in polynomial time," *SIAM J. Comput.* **31**, 1229–1254 (2002).
  - [6] Barbara M. Terhal and David P. DiVincenzo, "Classical simulation of noninteracting-fermion quantum circuits," *Phys. Rev. A* **65**, 032325 (2002).
  - [7] Scott Aaronson and Alex Arkhipov, "Bosonsampling is far from uniform," [arXiv:1309.7460](https://arxiv.org/abs/1309.7460) (2013).
  - [8] Michael Wimmer, "Algorithm 923: Efficient numerical computation of the pfaffian for dense and banded skew-symmetric matrices," *ACM T. Math. Software* **38**, 30 (2012).
  - [9] Norbert Schuch and Frank Verstraete, "Computational complexity of interacting electrons and fundamental limitations of density functional theory," *Nat. Phys.* **5**, 732–735 (2009).
  - [10] Richard Jozsa and Maarten Van den Nest, "Classical simulation complexity of extended clifford circuits," [arXiv:1305.6190](https://arxiv.org/abs/1305.6190) (2013).
  - [11] Bill Fefferman and Chris Umans, "The power of quantum fourier sampling," [arXiv:1507.05592](https://arxiv.org/abs/1507.05592) (2015).
  - [12] Michael J. Bremner, Ashley Montanaro, and Dan J. Shepherd, "Average-case complexity versus approximate simulation of commuting quantum computations," *Phys. Rev. Lett.* **117**, 080501 (2016).
  - [13] Abhinav Deshpande, Bill Fefferman, Minh C. Tran, Michael Foss-Feig, and Alexey V. Gorshkov, "Dynamical phase transitions in sampling complexity," *Phys. Rev. Lett.* **121**, 030501 (2018).
  - [14] Gopikrishnan Muraleedharan, Akimasa Miyake, and Ivan H. Deutsch, "Quantum computational supremacy in the sampling of bosonic random walkers on a one-dimensional lattice," *New J. Phys.* **21**, 055003 (2018).
  - [15] Heinz-Peter Breuer and Francesco Petruccione, *The theory of open quantum systems* (Oxford University Press, 2007).
  - [16] Tomaž Prosen, "Spectral theorem for the lindblad equation for quadratic open fermionic systems," *J. Stat. Mech.-Theory. E* **2010**, P07020 (2010).
  - [17] Sergey Bravyi and Robert König, "Classical simulation of dissipative fermionic linear optics," *Quantum Information & Computation* **12**, 925–943 (2012).
  - [18] Crispin Gardiner, Peter Zoller, and Peter Zoller, *Quantum noise*, Vol. 56 (Springer, 2004).
  - [19] Baidyanath Misra and EC George Sudarshan, "The zenos paradox in quantum theory," *J. Math. Phys.* **18**, 756–763

- (1977).
- [20] A. Degasperis, L. Fonda, and G. C. Ghirardi, “Does the lifetime of an unstable system depend on the measuring apparatus?” *Il Nuovo Cimento A (1965-1970)* **21**, 471–484 (1974).
  - [21] J. D. Franson, B. C. Jacobs, and T. B. Pittman, “Quantum computing using single photons and the zeno effect,” *Phys. Rev. A* **70**, 062302 (2004).
  - [22] Yu-Zhu Sun, Yu-Ping Huang, and Prem Kumar, “Photonic nonlinearities via quantum zeno blockade,” *Phys. Rev. Lett.* **110**, 223901 (2013).
  - [23] Andrew J. Daley, Martin M. Boyd, Jun Ye, and Peter Zoller, “Quantum computing with alkaline-earth-metal atoms,” *Phys. Rev. Lett.* **101**, 170504 (2008).
  - [24] Marco Anderlini, Patricia J. Lee, Benjamin L. Brown, Jennifer Sebby-Strabley, William D. Phillips, and J. V. Porto, “Controlled exchange interaction between pairs of neutral atoms in an optical lattice,” *Nature* **448**, 452–456 (2007).
  - [25] P. J. Lee, M. Anderlini, B. L. Brown, J. Sebby-Strabley, W. D. Phillips, and J. V. Porto, “Sublattice addressing and spin-dependent motion of atoms in a double-well lattice,” *Phys. Rev. Lett.* **99**, 020402 (2007).
  - [26] Chuanwei Zhang, S. L. Rolston, and S. Das Sarma, “Manipulation of single neutral atoms in optical lattices,” *Phys. Rev. A* **74**, 042316 (2006).
  - [27] A. D. Ludlow, N. D. Lemke, J. A. Sherman, C. W. Oates, G. Quémener, J. von Stecher, and A. M. Rey, “Cold-collision-shift cancellation and inelastic scattering in a yb optical lattice clock,” *Phys. Rev. A* **84**, 052724 (2011).
  - [28] Ren Zhang, Yanting Cheng, Hui Zhai, and Peng Zhang, “Orbital feshbach resonance in alkali-earth atoms,” *Phys. Rev. Lett.* **115**, 135301 (2015).
  - [29] L. Riegger, N. Darkwah Oppong, M. Höfer, D. R. Fernandes, I. Bloch, and S. Fölling, “Localized magnetic moments with tunable spin exchange in a gas of ultracold fermions,” *Phys. Rev. Lett.* **120**, 143601 (2018).
  - [30] F. Scazza, C. Hofrichter, M. Höfer, P. C. De Groot, I. Bloch, and S. Fölling, “Observation of two-orbital spin-exchange interactions with ultracold su(n)-symmetric fermions,” *Nat. Phys.* **10**, 779–784 (2014).
  - [31] Rodolphe Le Targat, Xavier Baillard, Mathilde Fouché, Anders Brusch, Olivier Tcherbakoff, Giovanni D. Rovera, and Pierre Lemonde, “Accurate optical lattice clock with  $^{87}\text{Sr}$  atoms,” *Phys. Rev. Lett.* **97**, 130801 (2006).
  - [32] G. Cappellini, L. F. Livi, L. Franchi, D. Tusi, D. Benedicto Orenes, M. Inguscio, J. Catani, and L. Fallani, “Coherent manipulation of orbital feshbach molecules of two-electron atoms,” *Phys. Rev. X* **9**, 011028 (2019).
  - [33] N. Syassen, D. M. Bauer, M. Lettner, T. Volz, D. Dietze, J. J. García-Ripoll, J. I. Cirac, G. Rempe, and S. Dürr, “Strong dissipation inhibits losses and induces correlations in cold molecular gases,” *Science* **320**, 1329–1331 (2008).
  - [34] Bo Yan, Steven A. Moses, Bryce Gadway, Jacob P. Covey, Kaden R. A. Hazzard, Ana Maria Rey, Deborah S. Jin, and Jun Ye, “Observation of dipolar spin-exchange interactions with lattice-confined polar molecules,” *Nature* **501**, 521 EP – (2013).
  - [35] Cheng Chin, Rudolf Grimm, Paul Julienne, and Eite Tiesinga, “Feshbach resonances in ultracold gases,” *Rev. Mod. Phys.* **82**, 1225–1286 (2010).
  - [36] S. Giorgini, L. P. Pitaevskii, and S. Stringari, “Theory of ultracold atomic fermi gases,” *Rev. Mod. Phys.* **80**, 1215–1274 (2008).
  - [37] G. Barontini, R. Labouvie, F. Stubenrauch, A. Vogler, V. Guarrera, and H. Ott, “Controlling the dynamics of an open many-body quantum system with localized dissipation,” *Phys. Rev. Lett.* **110**, 035302 (2013).
  - [38] Ralf Labouvie, Bodhaditya Santra, Simon Heun, Sandro Wimberger, and Herwig Ott, “Negative differential conductivity in an interacting quantum gas,” *Phys. Rev. Lett.* **115**, 050601 (2015).
  - [39] Ralf Labouvie, Bodhaditya Santra, Simon Heun, and Herwig Ott, “Bistability in a driven-dissipative superfluid,” *Phys. Rev. Lett.* **116**, 235302 (2016).
  - [40] Henrik P. Lüschen, Pranjal Bordia, Sean S. Hodgman, Michael Schreiber, Saubhik Sarkar, Andrew J. Daley, Mark H. Fischer, Ehud Altman, Immanuel Bloch, and Ulrich Schneider, “Signatures of many-body localization in a controlled open quantum system,” *Phys. Rev. X* **7**, 011034 (2017).
  - [41] Y. S. Patil, S. Chakram, and M. Vengalattore, “Measurement-induced localization of an ultracold lattice gas,” *Phys. Rev. Lett.* **115**, 140402 (2015).
  - [42] Jiaming Li, Andrew K. Harter, Ji Liu, Leonardo de Melo, Yogesh N. Joglekar, and Le Luo, “Observation of parity-time symmetry breaking transitions in a dissipative floquet system of ultracold atoms,” *Nat. Commun.* **10**, 855 (2019).
  - [43] R. Bonifacio, F. Casagrande, and M. Milani, “Superradiance and superfluorescence in josephson junction arrays,” *Phys. Lett. A* **101**, 427–431 (1984).
  - [44] M. C. Cassidy, A. Bruno, S. Rubbert, M. Irfan, J. Kammhuber, R. N. Schouten, A. R. Akhmerov, and L. P. Kouwenhoven, “Demonstration of an ac josephson junction laser,” *Science* **355**, 939–942 (2017).
  - [45] Tony E. Lee and Ching-Kit Chan, “Heralded magnetism in non-hermitian atomic systems,” *Phys. Rev. X* **4**, 041001 (2014).
  - [46] Tony E. Lee, Sarang Gopalakrishnan, and Mikhail D. Lukin, “Unconventional magnetism via optical pumping of interacting spin systems,” *Phys. Rev. Lett.* **110**, 257204 (2013).
  - [47] Chaitanya Joshi, Felix Nissen, and Jonathan Keeling, “Quantum correlations in the one-dimensional driven dissipative  $xy$  model,” *Phys. Rev. A* **88**, 063835 (2013).
  - [48] S. Diehl, W. Yi, A. J. Daley, and P. Zoller, “Dissipation-induced  $d$ -wave pairing of fermionic atoms in an optical lattice,” *Phys. Rev. Lett.* **105**, 227001 (2010).
  - [49] Kazuki Yamamoto, Masaya Nakagawa, Kyosuke Adachi, Kazuaki Takasan, Masahito Ueda, and Norio Kawakami, “Theory of non-hermitian fermionic superfluidity with a complex-valued interaction,” *Phys. Rev. Lett.* **123**, 123601 (2019).
  - [50] José A. S. Lourenço, Ronivon L. Eneias, and Rodrigo G. Pereira, “Kondo effect in a  $\mathcal{PT}$ -symmetric non-hermitian hamiltonian,” *Phys. Rev. B* **98**, 085126 (2018).
  - [51] Masaya Nakagawa, Norio Kawakami, and Masahito Ueda, “Non-hermitian kondo effect in ultracold alkaline-earth atoms,” *Phys. Rev. Lett.* **121**, 203001 (2018).
  - [52] M. S. Rudner and L. S. Levitov, “Topological transition in a non-hermitian quantum walk,” *Phys. Rev. Lett.* **102**, 065703 (2009).
  - [53] Tony E. Lee, “Anomalous edge state in a non-hermitian lattice,” *Phys. Rev. Lett.* **116**, 133903 (2016).
  - [54] Daniel Leykam, Konstantin Y. Bliokh, Chunli Huang, Y. D. Chong, and Franco Nori, “Edge modes, degeneracies, and topological numbers in non-hermitian systems,” *Phys. Rev. Lett.* **118**, 040401 (2017).
  - [55] Shunyu Yao and Zhong Wang, “Edge states and topological invariants of non-hermitian systems,” *Phys. Rev. Lett.* **121**, 086803 (2018).
  - [56] Zongping Gong, Yuto Ashida, Kohei Kawabata, Kazuaki

- Takasan, Sho Higashikawa, and Masahito Ueda, “Topological phases of non-hermitian systems,” *Phys. Rev. X* **8**, 031079 (2018).
- [57] Huitao Shen, Bo Zhen, and Liang Fu, “Topological band theory for non-hermitian hamiltonians,” *Phys. Rev. Lett.* **120**, 146402 (2018).
- [58] Kohei Kawabata, Ken Shiozaki, Masahito Ueda, and Masatoshi Sato, “Symmetry and topology in non-hermitian physics,” *Phys. Rev. X* **9**, 041015 (2019).
- [59] K. B. Efetov, “Directed quantum chaos,” *Phys. Rev. Lett.* **79**, 491–494 (1997).
- [60] Ilya Ya. Goldsheid and Boris A. Khoruzhenko, “Distribution of eigenvalues in non-hermitian anderson models,” *Phys. Rev. Lett.* **80**, 2897–2900 (1998).
- [61] Stefano Longhi, Davide Gatti, and Giuseppe Della Valle, “Non-hermitian transparency and one-way transport in low-dimensional lattices by an imaginary gauge field,” *Phys. Rev. B* **92**, 094204 (2015).
- [62] To be precise, for the first task (estimating few-body observables), the error is measured by the maximum difference in the estimated and ideal expectation values of a unit-norm observable  $O$ . For the second task (sampling), the error is measured through the maximum variation distance between the ideal and the sampled probability distributions.
- [63] G. Lindblad, “On the generators of quantum dynamical semigroups,” *Comm. Math. Phys.* **48**, 119–130 (1976).
- [64] Elsi-Mari Laine, Jyrki Piilo, and Heinz-Peter Breuer, “Measure for the non-markovianity of quantum processes,” *Phys. Rev. A* **81**, 062115 (2010).
- [65] JHP Colpa, “Diagonalisation of the quadratic fermion hamiltonian with a linear part,” *J. Phys. A-Math. Gen.* **12**, 469 (1979).
- [66] Michael S. Underwood and David L. Feder, “Bose-Hubbard model for universal quantum walk-based computation,” *Phys. Rev. A* **85**, 052314 (2012).
- [67] Scott Aaronson and Alex Arkhipov, “The computational complexity of linear optics,” in *Proceedings of the forty-third annual ACM symposium on Theory of computing* (ACM, 2011) pp. 333–342.
- [68] Adam Bouldan, Bill Fefferman, Chinmay Nirkhe, and Umesh Vazirani, “On the complexity and verification of quantum random circuit sampling,” *Nat. Phys.* **15**, 159–163 (2019).
- [69] Panos Aliferis and Barbara M. Terhal, “Fault-tolerant quantum computation for local leakage faults,” *Quantum Information & Computation* **7**, 139–156 (2007).
- [70] D. Aharonov and M. Ben-Or, “Fault-tolerant quantum computation with constant error,” in *Proceedings of the Twenty-Ninth Annual ACM Symposium on Theory of Computing - STOC '97* (ACM Press, El Paso, Texas, United States, 1997) pp. 176–188.
- [71] Emanuel Knill, Raymond Laflamme, and Wojciech H. Zurek, “Resilient quantum computation,” *Science* **279**, 342–345 (1998).
- [72] Barbara M. Terhal, “Quantum error correction for quantum memories,” *Rev. Mod. Phys.* **87**, 307–346 (2015).
- [73] E. Arimondo, M. Inguscio, and P. Violino, “Experimental determination of the hyperfine structure in the alkali atoms,” *Rev. Mod. Phys.* **49**, 31–76 (1977).
- [74] Stephan Falke, Horst Knöckel, Jan Friebe, Matthias Riedmann, Eberhard Tiemann, and Christian Lisdat, “Potassium ground-state scattering parameters and born-oppenheimer potentials from molecular spectroscopy,” *Phys. Rev. A* **78**, 012503 (2008).
- [75] H. T. C. Stoof, J. M. V. A. Koelman, and B. J. Verhaar, “Spin-exchange and dipole relaxation rates in atomic hydrogen: rigorous and simplified calculations,” *Phys. Rev. B* **38**, 4688–4697 (1988).
- [76] T. Loftus, C. A. Regal, C. Ticknor, J. L. Bohn, and D. S. Jin, “Resonant control of elastic collisions in an optically trapped fermi gas of atoms,” *Phys. Rev. Lett.* **88**, 173201 (2002).
- [77] C. A. Regal and D. S. Jin, “Measurement of positive and negative scattering lengths in a fermi gas of atoms,” *Phys. Rev. Lett.* **90**, 230404 (2003).
- [78] C. D’Errico, M. Zaccanti, M. Fattori, G. Roati, M. Inguscio, G. Modugno, and A. Simoni, “Feshbach resonances in ultracold  $^{39}\text{K}$ ,” *New J. Phys.* **9**, 223 (2007).
- [79] A. Ludewig, *Feshbach Resonances in  $^{40}\text{K}$* , Ph.D. thesis, University of Amsterdam (2012).
- [80] J. S. Krauser, J. Heinze, S. Götze, M. Langbecker, N. Fläschner, L. Cook, T. M. Hanna, E. Tiesinga, K. Sengstock, and C. Becker, “Investigation of feshbach resonances in ultracold  $^{40}\text{K}$  spin mixtures,” *Phys. Rev. A* **95**, 042701 (2017).
- [81] L. Tanzi, C. R. Cabrera, J. Sanz, P. Cheiney, M. Tomza, and L. Tarruell, “Feshbach resonances in potassium bose-bose mixtures,” *Phys. Rev. A* **98**, 062712 (2018).
- [82] Roman Chapurin, Xin Xie, Michael J. Van de Graaff, Jared S. Popowski, José P. D’Incao, Paul S. Julienne, Jun Ye, and Eric A. Cornell, “Precision test of the limits to universality in few-body physics,” *Phys. Rev. Lett.* **123**, 233402 (2019).
- [83] N. Balakrishnan, V. Kharchenko, R.C. Forrey, and A. Dalgarno, “Complex scattering lengths in multi-channel atom-molecule collisions,” *Chem. Phys. Lett.* **280**, 5 (1997).
- [84] J. L. Bohn and P. S. Julienne, “Prospects for influencing scattering lengths with far-off-resonant light,” *Phys. Rev. A* **56**, 1486–1491 (1997).
- [85] Jeremy M Hutson, “Feshbach resonances in ultracold atomic and molecular collisions: threshold behaviour and suppression of poles in scattering lengths,” *New J. Phys.* **9**, 152 (2007).
- [86] Zbigniew Idziaszek and Paul S. Julienne, “Universal Rate Constants for Reactive Collisions of Ultracold Molecules,” *Phys. Rev. Lett.* **104**, 113202 (2010).
- [87] Matthew D Frye, Paul S Julienne, and Jeremy M Hutson, “Cold atomic and molecular collisions: approaching the universal loss regime,” *New J. Phys.* **17**, 045019 (2015).
- [88] T. L. Nicholson, S. Blatt, B. J. Bloom, J. R. Williams, J. W. Thomsen, J. Ye, and Paul S. Julienne, “Optical feshbach resonances: Field-dressed theory and comparison with experiments,” *Phys. Rev. A* **92**, 022709 (2015).
- [89] K. Huang and T. D. Lee, “Quantum mechanical many-body problem with hard sphere interaction,” *Phys. Rev.* **105**, 767–775 (1957).
- [90] I. Bloch, “Ultracold quantum gases in optical lattices,” *Nat. Phys.* **1**, 23–30 (2005).
- [91] T Busch, B-G Englert, K Rzażewski, and M Wilkens, “Two cold atoms in a harmonic trap,” *Found. of Phys.* **28**, 549–559 (1998).
- [92] D. Blume and Chris H. Greene, “Fermi pseudopotential approximation: Two particles under external confinement,” *Phys. Rev. A* **65**, 043613 (2002).
- [93] E. L. Bolda, E. Tiesinga, and P. S. Julienne, “Effective-scattering-length model of ultracold atomic collisions and feshbach resonances in tight harmonic traps,” *Phys. Rev. A* **66** (2002).
- [94] E. Tiesinga, C. J. Williams, F. H. Mies, and P. S. Julienne, “Interacting atoms under strong quantum confinement,” *Phys. Rev. A* **61**, 063416 (2000).
- [95] B. DeMarco, J. L. Bohn, J. P. Burke, Jr., M. Holland, and D. S. Jin, “Measurement of  $p$ -wave threshold law using evap-



- oratively cooled fermionic atoms,” *Phys. Rev. Lett.* **82**, 4208 (1999).
- [96] C. A. Regal, C. Ticknor, J. L. Bohn, and D. S. Jin, “Tuning  $p$ -wave interactions in an ultracold fermi gas of atoms,” *Phys. Rev. Lett.* **90**, 053201 (2003).
- [97] Zbigniew Idziaszek and Tommaso Calarco, “Pseudopotential method for higher partial wave scattering,” *Phys. Rev. Lett.* **96**, 013201 (2006).
- [98] D. D. Yavuz, P. B. Kulatunga, E. Urban, T. A. Johnson, N. Proite, T. Henage, T. G. Walker, and M. Saffman, “Fast ground state manipulation of neutral atoms in microscopic optical traps,” *Phys. Rev. Lett.* **96**, 063001 (2006).
- [99] Alexey V. Gorshkov, Liang Jiang, Markus Greiner, Peter Zoller, and Mikhail D. Lukin, “Coherent quantum optical control with subwavelength resolution,” *Phys. Rev. Lett.* **100**, 093005 (2008).
- [100] K. D. Stokes, C. Schnurr, J. R. Gardner, M. Marable, G. R. Welch, and J. E. Thomas, “Precision position measurement of moving atoms using optical fields,” *Phys. Rev. Lett.* **67**, 1997–2000 (1991).
- [101] D. Schrader, I. Dotsenko, M. Khudaverdyan, Y. Miroshnychenko, A. Rauschenbeutel, and D. Meschede, “Neutral atom quantum register,” *Phys. Rev. Lett.* **93**, 150501 (2004).
- [102] J. R. Gardner, M. L. Marable, G. R. Welch, and J. E. Thomas, “Suboptical wavelength position measurement of moving atoms using optical fields,” *Phys. Rev. Lett.* **70**, 3404–3407 (1993).
- [103] D. D. Yavuz and N. A. Proite, “Nanoscale resolution fluorescence microscopy using electromagnetically induced transparency,” *Phys. Rev. A* **76**, 041802 (2007).
- [104] Tobias Tiecke, *Feshbach resonances in ultracold mixtures of the fermionic quantum gases*, Ph.D. thesis (2009).
- [105] Martin Hebenstreit, Richard Jozsa, Barbara Kraus, Sergii Strelchuk, and Mithuna Yoganathan, “All pure fermionic non-Gaussian states are magic states for matchgate computations,” *Phys. Rev. Lett.* **123**, 080503 (2019).
- [106] Nishad Maskara, Abhinav Deshpande, Minh C. Tran, Adam Ehrenberg, Bill Fefferman, and Alexey V. Gorshkov, “Complexity phase diagram for interacting and long-range bosonic Hamiltonians,” (2019), [arXiv:1906.04178](https://arxiv.org/abs/1906.04178).
- [107] Ramis Movassagh, “Cayley path and quantum computational supremacy: A proof of average-case  $\#P$ -hardness of Random Circuit Sampling with quantified robustness,” (2019), [arXiv:1909.06210](https://arxiv.org/abs/1909.06210).